



HAL
open science

From mononuclear iron phthalocyanines in catalysis to μ -nitrido diiron complexes and beyond

A. B. Sorokin

► **To cite this version:**

A. B. Sorokin. From mononuclear iron phthalocyanines in catalysis to μ -nitrido diiron complexes and beyond. *Catalysis Today*, 2021, 373, pp.38-58. 10.1016/j.cattod.2021.03.016 . hal-03430670

HAL Id: hal-03430670

<https://hal.science/hal-03430670v1>

Submitted on 16 Nov 2021

HAL is a multi-disciplinary open access archive for the deposit and dissemination of scientific research documents, whether they are published or not. The documents may come from teaching and research institutions in France or abroad, or from public or private research centers.

L'archive ouverte pluridisciplinaire **HAL**, est destinée au dépôt et à la diffusion de documents scientifiques de niveau recherche, publiés ou non, émanant des établissements d'enseignement et de recherche français ou étrangers, des laboratoires publics ou privés.

From mononuclear iron phthalocyanines in catalysis to μ -nitrido diiron complexes and beyond

Alexander B. Sorokin^{a*}

^a Institut de Recherches sur la Catalyse et l'Environnement de Lyon (IRCELYON), UMR 5256, CNRS-Université Lyon 1, 2, av. A. Einstein, 69626 Villeurbanne Cedex, France

Fax: (+33) 472 445 399; phone: (+33) 472 445 337;

e-mail: alexander.sorokin@ircelyon.univ-lyon1.fr

Abstract For a long time biomimetic oxidation catalysis was mainly associated with metal porphyrin complexes. Phthalocyanine complexes, also belonging to large family of macrocyclic complexes have been under-investigated as catalysts until recently. In this review, we present the development of phthalocyanine catalytic chemistry at IRCELYON with a topical focus on contributions from our group during last 20 years and discuss recent research directions from personal perspective. Catalytic chemistry of phthalocyanine complexes is a rapidly growing field including not only oxidations but also many other reactions. Recent discovery of remarkable catalytic properties of μ -nitrido diiron phthalocyanines will give a new impetus and should even accelerate this development. These binuclear N-bridged complexes emerge as promising bio-inspired catalysts, in particular, for challenging reactions such as a low temperature oxidation of methane and oxidative defluorination of heavily fluorinated aromatic compounds. The scope of their catalytic applications is constantly increasing. The bimetallic construction is flexible and has a significant potential for further development including implementation of different ligands, metals and bridging groups. Consequently, the properties of this scaffold can be fine-tuned by platform architecture thus providing novel tools for catalysis.

Keywords: oxidation, catalysis, phthalocyanine, μ -nitrido, binuclear complexes; bio-inspired.

1. Introduction

Enzymes containing iron porphyrin active sites are involved in essential processes in living organisms and catalyze a variety of chemical reactions with extremely high efficiency and selectivity. Outstanding catalytic properties of cytochrome P450 in many reactions including mild and selective oxidation of strong C-H bonds of alkanes have initiated an extensive research on biomimetic oxidation since 1980s with particular emphasis on porphyrin complexes [1]. A large variety of synthetic porphyrin complexes have been designed in order to mimic remarkable reactivity of cytochrome P450 and to create efficient chemical systems for oxidation and other reactions [2-4]. Some other tetrapyrrolic macrocyclic complexes, e.g., phthalocyanines [5] and corroles [6], have been investigated in bio-inspired catalysis to a much lesser extent.

During my postdoctoral stay with Bernard Meunier at Laboratoire de Chimie de Coordination in Toulouse we decided to evaluate iron phthalocyanine complexes as catalysts for degradation of chlorinated phenols since these complexes are readily available in industrial scale and hence more attractive than porphyrin complexes from application perspective. We have introduced iron 2,9(10),16(17),23(24)-tetrasulfophthalocyanine (FePcS, the structure is shown in Fig. 1) as a very active catalyst for the oxidative degradation of recalcitrant priority pollutants, such as 2,4,6-trichlorophenol (TCP) and other chlorinated phenols [7-10] as well as for other pollutants [11-13].

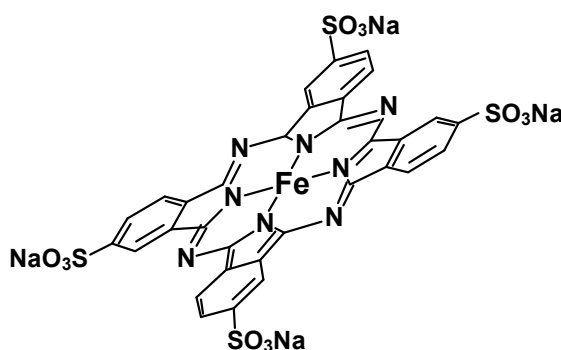


Fig. 1. Structure of iron 2,9(10),16(17),23(24)-tetrasulfophthalocyanine (FePcS).

This research direction has been further developed by many researchers toward degradation of different pollutants using a variety of phthalocyanine metal complexes [14-26].

Although metal phthalocyanine complexes (MPc) are efficient catalysts for other reactions [27] including selective oxidations and bleaching [28] their catalytic chemistry in terms of reactivity scope and reaction mechanisms as well as active species involved was largely under-developed at that time as compared to porphyrin counterparts.

In 1998, I have started my independent research at IRCELYON focused to the development of novel catalytic methods based on MPc complexes and also to mechanistic studies, detection and characterization of active species involved in the catalysis. We have prepared the first high-valent iron oxo complex from FePc^tBu₄ and m-chloroperbenzoic acid (m-CPBA) at -60°C thus confirming that phthalocyanine complexes exhibit mechanistic paradigm similar to their porphyrin counterparts [29]. This transient species was characterized by UV-vis, cryospray mass spectrometry, EPR, X-ray absorption and high-resolution X-ray emission techniques.

Among catalytic applications, the oxidation of polysaccharides appears to be particularly promising. Water soluble and readily available FePcS is an efficient homogeneous catalyst operating in less than 0.01 mol% loading for the clean oxidative transformation of starch and other polysaccharides to introduce both carboxyl and carbonyl groups to biopolymer backbone (typically 1-20 of each functionality per 100 anhydroglucose units) [30,31]. Carboxyl groups provide desired balance of hydrophilic/hydrophobic properties and possible solubility in water whereas carbonyl functions allow further grafting the different molecules to furnish materials with special properties. The practical one-pot process in water avoiding large energy consumption, separation steps and wastes affords elaborated biopolymers with tailored properties which can be useful in different applications, in particular, in cosmetic and paint formulations, paper and textile industries.

Another research project was directed to selective oxidation of aromatics and phenols to corresponding quinones using heterogeneous FePc-based catalysts. Aiming to support iron phthalocyanine in a priori active mononuclear form, we have treated as-synthesized FePcS

composed mainly of μ -oxo dimer by SOCl_2 or PCl_5 to get $\text{FePc}(\text{SO}_2\text{Cl})_4$ material suitable for covalent anchoring to amino-modified mesoporous silicas. When we used a freshly prepared $\text{FePc}(\text{SO}_2\text{Cl})_4$ solution in pyridine, a blue solid material was obtained after grafting. The diffuse reflectance UV-vis spectrum of supported material showed Q band at 636 nm with a small shoulder at 690 nm indicating μ -oxo dimer as a major anchored species and only small amount of grafted monomeric FePcS complex (Fig. 2).

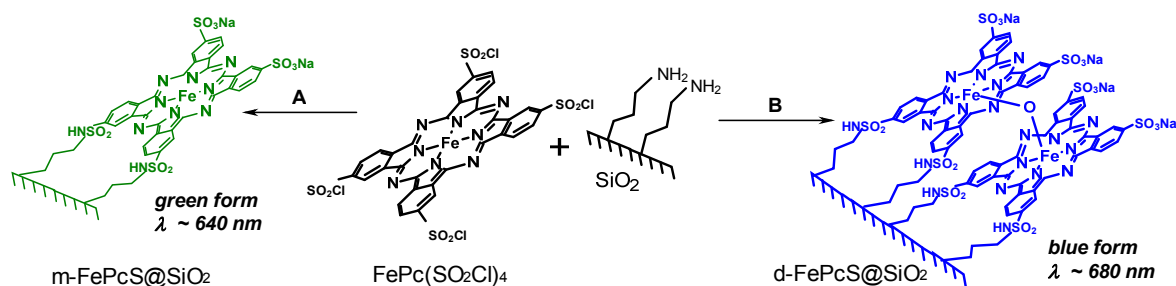


Fig. 2. Covalent grafting of FePcS onto silicas in monomeric and dimeric forms.

We were aware that such dimeric species have been generally considered by catalytic chemists as inactive in catalysis, therefore we tried to support FePcS in monomeric rather than in dimeric form. Preliminary incubation of $\text{FePc}(\text{SO}_2\text{Cl})_4$ solution in pyridine for 18 h provided mononuclear dipyrindine complex which was successfully grafted to amino-modified MCM-41 in monomeric form as attested by Q band at 682 nm in the UV-vis spectrum. Surprisingly, this target monomeric catalyst was rather poor catalyst in the oxidation of 2-methylnaphthalene (2MN) and 2,3,6-trimethylphenol (TMP) to corresponding quinones (Fig. 3).

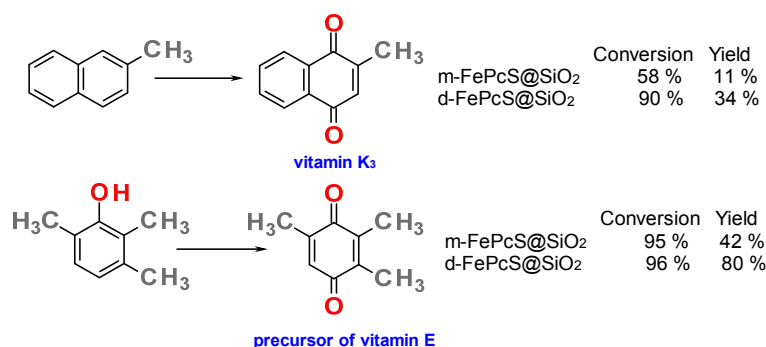


Fig. 3. Comparison of monomeric m-FePcS@SiO_2 and dimeric d-FePcS@SiO_2 catalysts in the oxidation of 2-methylnaphthalene and 2,3,6-trimethylphenol by $^t\text{BuOOH}$.

Unexpectedly, the supported catalyst containing principally μ -oxo dimer $(\text{FePcS})_2\text{O}$ exhibited notably higher activity and selectivity providing 2-methyl-naphthaquinone (2MQ) and trimethylbenzoquinone (TMQ) with 34 and 80 % yields, respectively (Fig. 3). The d-FePcS@SiO_2 catalyst retained the catalytic activity in TMP oxidation during 3 successive runs, but the selectivity has progressively diminished from 80 to 51 %. The UV-vis spectrum of the solid recovered after third run showed a sharp band at 688 nm indicating monomeric FePcS as principal grafted species. Thus, during catalysis the selective dimeric species were gradually transformed to less selective monomeric species thus indicating the instability of μ -oxo diiron unit to monomerization.

The relative stabilization of the dimeric structure of supported phthalocyanine complexes has been achieved by covalent linking of two adjacent phthalocyanine molecules through an appropriate spacer, *N,N'*-diethyl-1,3-propanediamine (Fig. 4) [33].

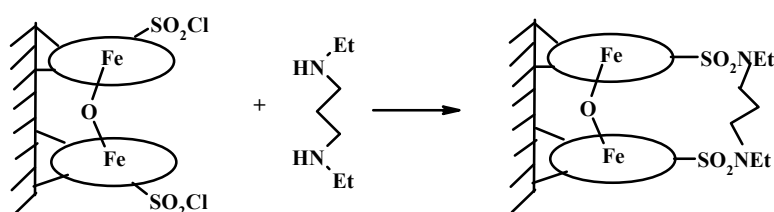


Fig. 4. Stabilization of dimeric structure by covalent linking of phthalocyanine moieties with *N,N'*-diethyl-1,3-propanediamine.

Indeed, the yield of TMQ was improved to 88 % thus confirming unexpectedly superior catalytic properties of μ -oxo iron dimer in oxidation. The excellent catalytic activity of μ -oxo diiron phthalocyanine complexes in the oxidation of aromatic compounds was further confirmed by Nemykin and coworkers [34-36].

Unforeseen catalytic activity of μ -oxo diiron phthalocyanine complexes can be rationalized as follows. First, the iron center coordinates the peroxide oxidant to form iron-peroxo complex (Fig. 5).

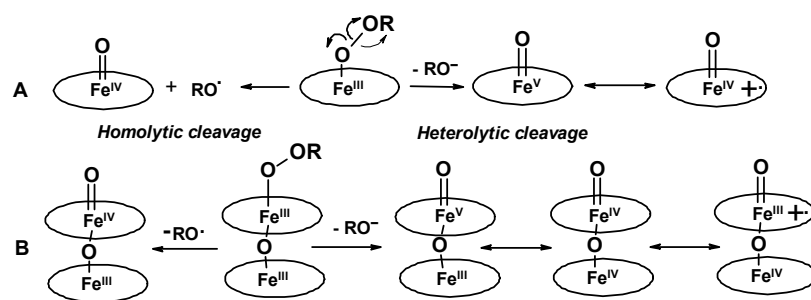


Fig. 5. Proposed mechanisms of the formation of active species from monomeric and dimeric μ -oxo macrocyclic complexes.

This complex can undergo either homolytic or heterolytic cleavages of the O-O bond depending on the macrocycle and peroxide structures, presence and nature of axial ligand, solvent polarity [27]. Homolysis of O-O bond in mononuclear (L)Fe^{III}-O-OR to form (L)Fe^{IV}=O and [•]OR is often the principal pathway leading to unselective free radical chemistry (Fig. 5A). The heterolytic O-O cleavage leads to generation of high-valent active oxo species where the iron site(s) increases their oxidation state by two redox equivalents. This high oxidation state is stabilized by charge delocalization at iron site and macrocyclic ligand in mononuclear (L⁺)Fe^{IV}=O species and at two iron sites and two macrocyclic ligands in corresponding oxo species at μ -oxo diiron platform (Fig. 5B). Therefore, a desired higher valent oxo species with stronger oxidizing properties are more accessible at dimeric platform. Thus, diiron macrocyclic construction provides better possibilities for delocalization of the high positive charge during formation of active oxidizing species that can be advantageously used in the oxidation catalysis despite the general belief in the catalytic inertness of dimeric macrocyclic complexes.

Using ¹⁸O labeling and kinetic isotope effect studies [37], detailed analyses of the reaction products as well as kinetic and spectroscopic studies [38], the mechanism of selective oxidation of phenols involving μ -oxo diiron species was proposed (Fig. 6).

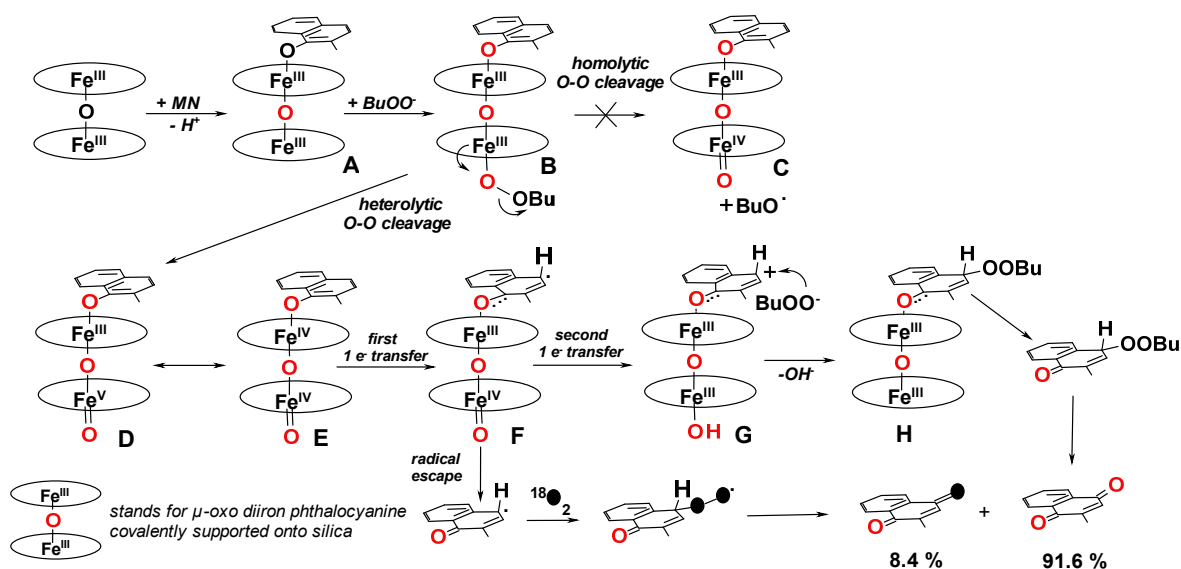


Fig. 6. Proposed mechanism of the oxidation of 2-methyl-naphthol by $t\text{BuOOH}$ catalyzed by supported $(\text{FePcS})_2\text{O}$ [38].

In the first step the coordination of phenol with supported μ -oxo diiron phthalocyanine occurs which is in agreement with UV-vis and kinetic data (near-zero order in TMP oxidation). Then, the phenolate complex **A** coordinates $t\text{BuOO}^-$ to form peroxo-intermediate **B** followed by either homolytic or heterolytic O-O bond cleavage. The homolytic cleavage of O-O bond would produce the $t\text{BuO}^\cdot$ radical. Yet, the low incorporation of ^{18}O in 2MQ in the presence $^{18}\text{O}_2$, the increase of the selectivity to 2MQ upon increasing the phenol concentration and the lack of EPR-detected radicals in the presence of the radical trap 3,5-dibromo-4-nitrosobenzenesulfonic acid (DBNBS) strongly suggest that homolytic cleavage of peroxo bond in **B** to form intermediate **C** hardly contributes to reaction pathway. Heterolysis of O-O bond in **B** generates $\text{Fe}^{\text{III}}\text{Fe}^{\text{V}}$ intermediate **D** existing in $\text{Fe}^{\text{IV}}\text{Fe}^{\text{IV}}$ form **E** due to delocalisation of the charge on two Fe ions resulting in the stabilization of the high-valent species. An intramolecular $1 e^-$ transfer in the intermediate **E** should lead to the radical species **F**. The escape of naphthol radical from **F** can be trapped by dioxygen that was observed in $^{18}\text{O}_2$ trapping experiment. Quinone labeled at one carbonyl position represents only 8.4 % of products indicating that this pathway should be minor one. In addition, naphthol radical should produce binaphthol via bimolecular oxidative coupling but we were unable to detect the coupling product(s). The second one-electron transfer in **F** can

lead to cationic species **G** which can undergo a nucleophilic attack of ${}^t\text{BuOO}^-$ to produce **H** leading to quinone 2MQ.

Supported diiron phthalocyanine catalysts have been further developed for synthetically useful aromatic oxidation of phenols bearing alcohol and double bonds to functionalized quinones [39]. Nevertheless, the intrinsic instability of μ -oxo diiron structural unit was the important limitation for further catalytic development. We have hypothesized that other binuclear platforms might also be of interest as catalysts and have extended our studies to other single-atom bridged complexes.

2. μ -Nitrido diiron phthalocyanines as novel class of bio-inspired catalysts

Apart from μ -oxo dimers, single-atom bridged metal complexes include μ -nitrido and μ -carbido species. The nature of the bridge determines the iron oxidation state. The neutral μ -oxo, μ -nitrido and μ -carbido diiron complexes are Fe(III)-O-Fe(III) , Fe(III)-N=Fe(IV) and Fe(IV)=C=Fe(IV) entities (Fig. 7).

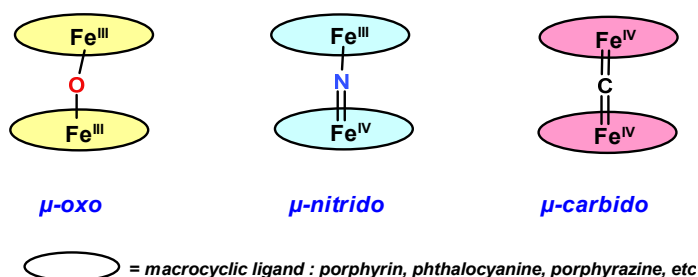


Fig. 7. Oxidation state of iron in single-atom bridged diiron porphyrinoid complexes.

The early studies of the single-atom bridged dimers focused to the synthetic developments and spectroscopic characterizations of these particular complexes [40-48] were nicely reviewed by Ercolani and coworkers [49]. The formally $\text{Fe(III)-}\mu\text{N-Fe(IV)}$ complexes containing one unpaired electron exhibit typical $S = \frac{1}{2}$ axial EPR spectra with weak or undetectable hyperfine splitting from the nitrogen bridge. However, a single doublet signal in their Mössbauer spectra indicates two equivalent iron centers in +3.5 oxidation state and μ -nitrido diiron species should be regarded as $\text{Fe(+3.5)-}\mu\text{N-Fe(+3.5)}$ systems [49]. While Fe(III)-

$\mu\text{O-Fe(III)}$ dimers contain antiferromagnetically coupled high-spin centers, $\text{Fe(+3.5)-}\mu\text{N-Fe(+3.5)}$ and $\text{Fe(IV)-}\mu\text{N-Fe(IV)}$ species are low-spin systems [50]. The structures of μ -nitrido diiron phthalocyanine and porphyrin complexes are shown in Fig. 8.

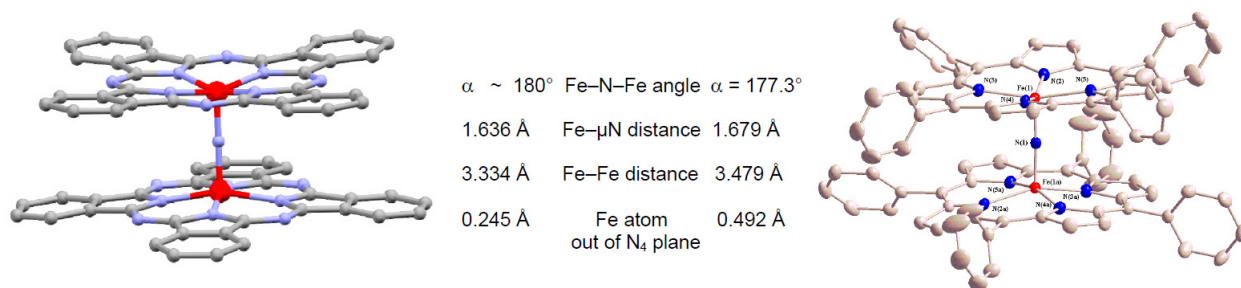


Fig. 8. Structures and principal geometrical parameters of μ -nitrido diiron phthalocyanine (left) and tetraphenylporphyrin (right) complexes.

Contrary to μ -oxo analogs, μ -nitrido diiron phthalocyanine complexes maintain the dimeric structure under acidic conditions and during the formation of high-valent species (*vide infra*). The structure of these bio-inspired complexes combines the features of two of the most powerful monooxygenase enzymes: diiron active site like in soluble methane monooxygenase and porphyrinoid supporting ligand similarly to iron porphyrin active site in cytochrome P-450. Compared to mononuclear counterparts, this binuclear scaffold provides better stabilization of high oxidation states of the catalyst developed during catalytic oxidation cycle [27].

It is worth noting that before our work μ -nitrido bimetallic complexes have not been considered as potential catalysts. We were delighted to observe unprecedented oxidative reactivity of μ -nitrido diiron tetra-*t*-butylphthalocyanine ($\text{FePc}^t\text{Bu}_4)_2\text{N}$ in very first experiments and further development led to the discovery of the remarkable catalytic properties of μ -nitrido diiron phthalocyanines in the oxidation of organic compounds, formation of C–C bonds and oxidative dehalogenation [51–59]. Detailed spectroscopic characterization of μ -nitrido diiron phthalocyanines and porphyrins and their high-valent species responsible for their high reactivity as well as comprehensive perspective of the range of catalytic applications can be found in the original articles [51–59] and recent reviews [60–62]. Below, we present selected catalytic

applications of μ -nitrido diiron phthalocyanines in challenging oxidations of methane, benzene and defluorination of poly- and perfluorinated aromatic compounds as well as recent catalytic developments. Then we describe related binuclear macrocyclic complexes with different bridging groups and their properties. Finally, we discuss future directions and trends for the further development of this class of catalysts.

3. Selected catalytic application of μ -nitrido diiron complexes

Strong oxidizing properties of cytochrome P450 with iron porphyrin site and diiron soluble methane monooxygenase are associated with their ability to generate high-valent oxo species such as Compound I with (porphyrin)⁺Fe^{IV}=O formulation. Such species with two redox equivalents above resting Fe(III) state are powerful oxidants though Compound I is not able to oxidize methane. Therefore, the ability to generate high-valent oxo species on μ -nitrido diiron platform is the prerequisite for their use in biomimetic oxidation catalysis. The μ -nitrido diiron structure is very stable due to the nitrogen bridging group and can stabilize high iron oxidation states [49,54,56]. However, the Fe^{+3.5}Fe^{+3.5} initial oxidation state in μ -nitrido diiron complexes appears to be not favorable for the activation of peroxides to form high-valent oxo species. Noteworthy, monooxygenase enzymes and regular biomimetic complexes form high-valent active oxo species at iron sites in low oxidation states [1]. Thus, the (L)Fe^{II} or (L)Fe^{III} sites are converted to (L)Fe^{IV}=O or (L)Fe^V=O / (L⁺)Fe^{IV}=O species with two redox equivalents above the initial Fe^{II} or Fe^{III} states, respectively (Fig. 9).

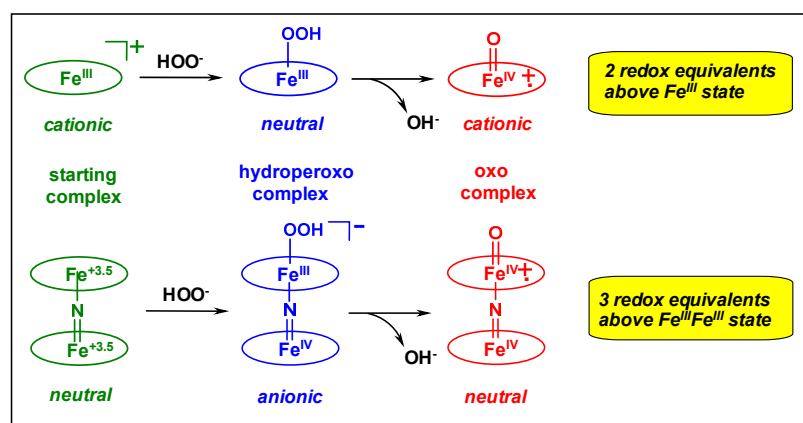


Fig. 9. Formation of oxo species on the mononuclear and binuclear platforms. Reprinted with permission from *Acc. Chem. Rev.* 49 (2016) 583-593. Copyright 2016 American Chemical Society.

The formation of high-valent oxo species appears to be harder starting with $\text{Fe}^{+3.5}\text{Fe}^{+3.5}$ entities since it is more difficult to remove two electrons from this already oxidized unit. However, if such species would be accessible, they might be even more powerful oxidants compared to their mononuclear counterparts because of their ultra-high oxidation state with 3 redox equivalents above Fe(III)Fe(III) state. We have succeeded to accomplish the formation of these μ -nitrido diiron oxo complexes and to characterize them by several spectroscopic techniques [51,60,61,63]. Their particular electronic structure differentiates them from corresponding mononuclear iron counterparts [64] and confers to them unprecedented catalytic properties which will be described below.

3.1. Oxidation of methane and ethane

We have demonstrated that a μ -nitrido high-valent diiron oxo complex supported by tetraphenylporphyrin ligand obtained using *m*-chloroperbenzoic acid as active oxygen donor was much stronger oxidant in the oxidation of alkanes including methane compared to its mononuclear analog [63]. However, from practical and environmental perspectives, H_2O_2 is the preferable oxidant excepting dioxygen. Therefore, the oxidation of methane by H_2O_2 was probed using μ -nitrido diiron phthalocyanines which are more industrially relevant compared to porphyrin counterparts. Homogeneous oxidation of methane in MeCN by the $(\text{FePc}^t\text{Bu}_4)_2\text{N}-\text{H}_2\text{O}_2$ system afforded formic acid as the principal product along with the minor amounts of methanol and formaldehyde [51,52]. However, organic solvent containing C-H bonds can also be oxidized in the presence of active species strong enough to oxidize methane. Thus, it cannot be excluded that the C_1 products could be also obtained from the oxidation of CH_3CN and their origin should be checked in labeling experiments using deuterated solvents and labeled $^{13}\text{CH}_4$.

To discriminate between methane oxidation and possible oxidation of acetonitrile, the oxidation was performed in CD₃CN. The GC-MS analysis of isotopic composition of formic acid revealed the presence of 68 % HCOOH and 32 % DCOOH, thus indicating parallel oxidation of CH₄ and CD₃CN, respectively (Fig. 10).

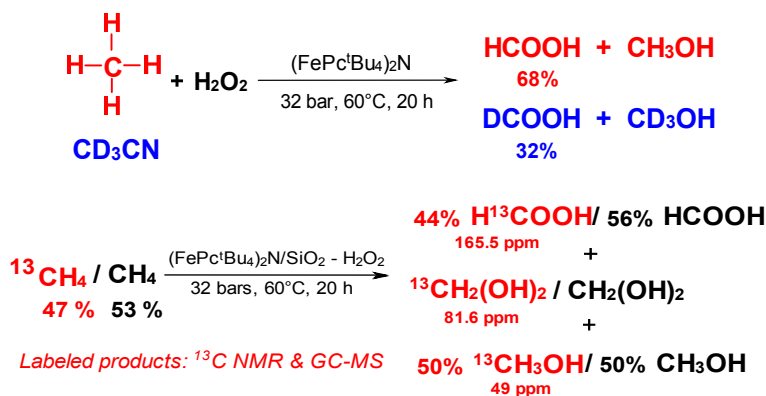


Fig. 10. Homogeneous oxidation of methane by the (FePc^tBu₄)₂N-H₂O₂ system in CD₃CN and heterogeneous oxidation of ¹³C-labeled methane by (FePc^tBu₄)₂N/SiO₂-H₂O₂ system. Reprinted with permission from Acc. Chem. Rev. 49 (2016) 583-593. Copyright 2016 American Chemical Society.

Indeed, formic acid principally originates from the methane oxidation with TON = 41 but the process is complicated by the oxidation of the solvent. To circumvent this problem, the oxidation of methane was run in water using silica-supported catalyst (20 μmol/g (FePc^tBu₄)₂N loading, 185 m²/g). When labelled ¹³CH₄ was employed, the formation of labelled ¹³CH₃OH, ¹³CH₂O and H¹³COOH unambiguously evidenced the occurrence of methane oxidation (Fig. 10). The preferential formation of formic acid can be explained by over-oxidation of initially formed CH₃OH and CH₂O in concentrations which are comparable with that of diluted CH₄. Notably, CH₄ can be oxidized by (FePc^tBu₄)₂N/SiO₂-H₂O₂ system in pure water at 25°C yet with a modest TON of 13. Performing the reaction at 40-60°C led to increase of TON up to 26-29.

Considerable enhancement of the catalytic efficiency was achieved upon lowering pH [51,52]. The protonation of coordinated peroxo group of (Pc)Fe^{IV}(μ-N)Fe^{III}(Pc)-O-OH promotes

heterolytic cleavage of O-O bond and formation of the active oxo species $(\text{Pc})\text{Fe}^{\text{IV}}(\mu\text{-N})\text{Fe}^{\text{IV}}(\text{Pc}^+)=\text{O}$ (Fig. 11).

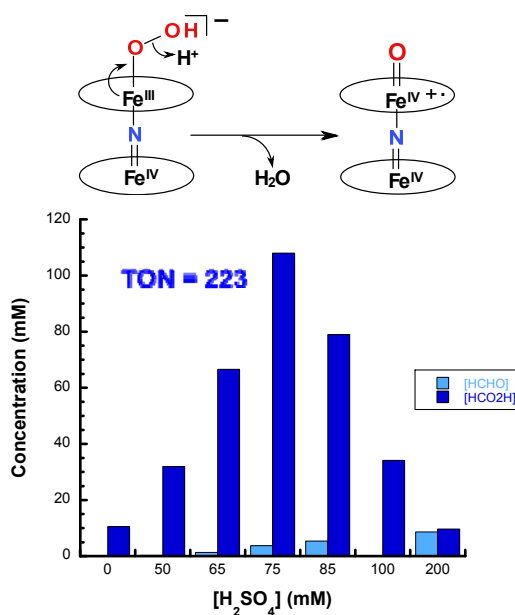


Fig. 11. Proton-assisted formation of active $(\text{Pc})\text{Fe}^{\text{IV}}(\mu\text{-N})\text{Fe}^{\text{IV}}(\text{Pc}^+)=\text{O}$ and efficiency of methane oxidation as function of H_2SO_4 concentration. Reaction conditions: methane (32 bar), 2 mL of aqueous solution, 0.925 μmol of supported FePc^tBu_4 catalyst, 678 μmol H_2O_2 , reaction time – 20 h. Adapted with permission from ref. 60. Copyright (2016) American Chemical Society.

The efficiency of the oxidation of methane revealed a bell-shaped dependence on the H_2SO_4 concentration with the highest catalytic activity at $[\text{H}_2\text{SO}_4] = 75 \text{ mM}$ (Fig. 11). Methane was converted to formic acid with TON up to 223 and 88-97% selectivity at 60°C. Importantly, the stability of supported catalyst was strongly improved in 75 mM H_2SO_4 and $(\text{FePc}^t\text{Bu}_4)_2\text{N}/\text{SiO}_2$ could be used in three successive methane oxidations to achieve a total TON=492, i.e. 492 methane molecules was oxidized by each $(\text{FePc}^t\text{Bu}_4)_2\text{N}$ molecule. Noteworthy, the catalytic activity of the $(\text{FePc}^t\text{Bu}_4)_2\text{N}/\text{SiO}_2\text{-H}_2\text{O}_2$ system in 75 mM H_2SO_4 aqueous solution at 25°C reached TON = 52 compared with TON = 13 in pure water.

The catalyst structure also influences the efficiency of methane oxidation. To gain insight into the electronic and structural features governing the formation of high-valent diiron oxo

species and their reactivity, two heteroleptic μ -nitrido dimers with distinct iron centers were synthesized [64]. One iron phthalocyanine bearing four or eight electron-withdrawing alkylsulfonyl groups was combined with more electron-rich iron unsubstituted phthalocyanine. This diiron scaffold allows probing the reactivity of two iron sites in the intramolecular fashion due to the formation of two isomeric $\text{Fe}(\mu\text{N})\text{Fe}=\text{O}$ species (Fig. 12).

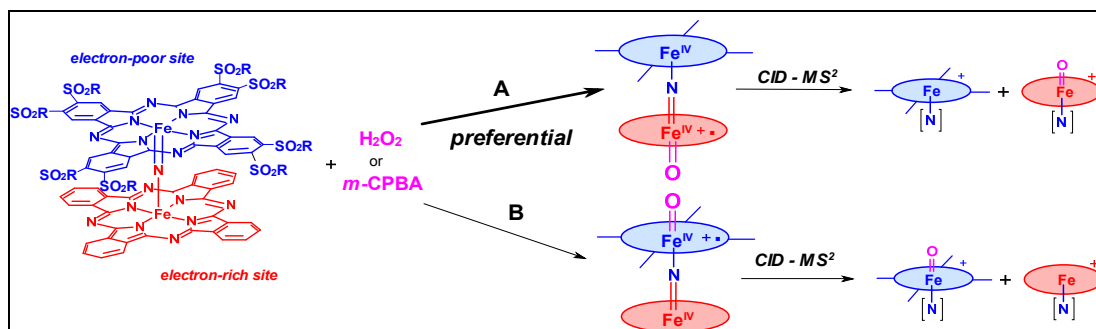


Fig. 12. Formation of two isomeric diiron oxo species at heteroleptic $(\text{PcSO}_2\text{R}_8)\text{Fe}(\mu\text{N})\text{Fe}(\text{Pc})$ platform and intramolecular determination of the position of oxo group by CID-MS/MS. Reprinted with permission from ref. 61. Copyright (2017) Elsevier.

Indeed, can non-equivalence of iron sites coordinated to ligands with different electronic properties cause the difference in the formation of the oxo species? We have studied in details the reactions of two heteroleptic complexes, $(\text{PcSO}_2\text{R}_8)\text{Fe}(\mu\text{N})\text{Fe}(\text{Pc})$ and $(\text{PcSO}_2\text{R}_4)\text{Fe}(\mu\text{N})\text{Fe}(\text{Pc})$, with two oxidants (H_2O_2 and $m\text{-CPBA}$) by mass spectrometry and DFT calculations [64]. These studies revealed the strong influence of the electronic properties of the iron center on the formation of $\text{Fe}(\mu\text{N})\text{Fe}=\text{O}$ species. The complex was rapidly reacted with oxidant at low temperature and the reaction mixture was analyzed using cold spray technique. Transient diiron oxo species were trapped in the quadrupole part of mass spectrometer and were subjected to collision induced dissociation tandem MS-MS fragmentation (CID-MS/MS). Dissociation of the $\text{Fe}(\mu\text{N})\text{Fe}=\text{O}$ molecular ions resulted in the monomeric fragments bearing oxo and nitrogen atoms (Fig. 12). Analysis of the fragmentation pattern and DFT calculations indicated that in all studied cases oxo group was situated at more electron-rich iron site (pathway

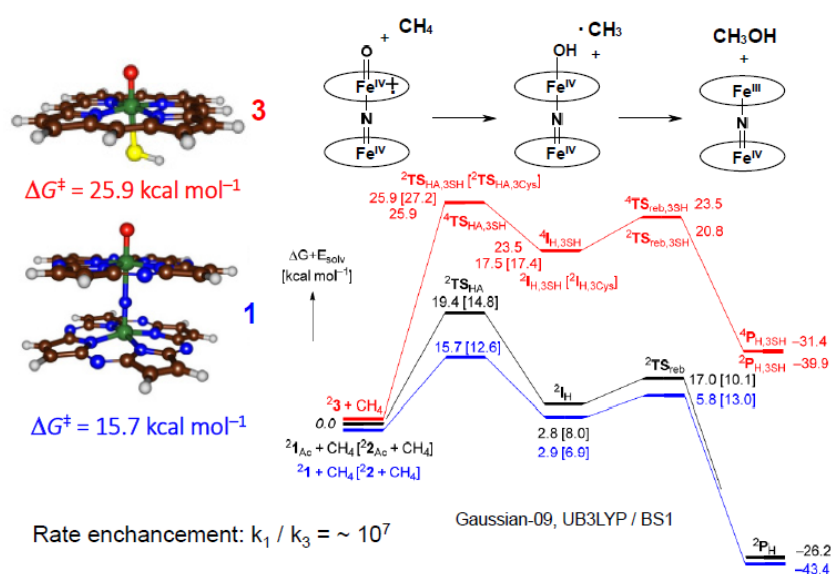


Fig. 14. DFT calculated methane hydroxylation pathway by μ -nitrido diiron oxo species (**1**) and by cytochrome P450 Compound I (**3**). Adapted with permission from ref. 66 (<https://pubs.acs.org/doi/10.1021/acscatal.5b02720>). Copyright (2016) American Chemical Society. Further permissions related to the material excerpted should be directed to the ACS.

Remarkably, these binuclear oxo species react with a free energy of activation that is ~ 10 kcal mol⁻¹ lower than that found for cytochrome P450 Compound I, which is one of the most reactive C-H oxidation species in Nature. The reactivity of the oxidizing species is related to the orbital mixing patterns along the Fe-O axis through which μ -N-Fe(IV) unit can donate electronic density to oxygen atom. This influences the pK_a of the oxo group and, consequently, the strength of the O-H bond in Fe^{IV}(μ N)Fe^{IV}-OH complex formed in the rate-determining step of hydrogen atom abstraction from methane [66]. The more electron-rich ligand is the higher the basicity of the oxo group and hence the more is the driving force of H-atom abstraction.

It is of great interest to determine how the nature of metal sites in μ -nitrido binuclear fragment might influence on the catalytic properties. De Visser and co-workers have performed computational studies on a μ -nitrido bridged diruthenium (IV) porphyrazine oxo species as well as its reaction with methane in comparison with corresponding diiron complex [67]. Both complexes are in a doublet spin ground state which is well-separated from other spin states and

oxo group has significant radical character. Although, the electronic configurations of oxo species of μ -nitrido diruthenium(IV) and diiron(IV) complexes are similar, the former reacts with methane with H-atom abstraction barrier that is considerably lower in energy (by ~ 5 kcal mol⁻¹). The diruthenium(IV)-oxo and diiron(IV)-oxo species exhibit similar spin and charge distributions, but the strength of the O-H bond formed is much stronger for Ru complex that should result in high reactivity of diruthenium species compared with its diiron counterpart [67].

The high reactivity of the μ -nitrido diiron phthalocyanine - H₂O₂ system in the oxidation of strong C-H bonds and high selectivity to acids was utilized for the direct oxidation of ethane to acetic acid [68]. The unsubstituted phthalocyanine complex (FePc)₂N supported onto SiO₂ exhibited promising results in the oxidation of ethane by H₂O₂ in water. Acetic acid was obtained with 71 % selectivity and turnover number of 58.

3.2. μ -N supramolecular conjugates for the oxidation of light alkanes

Recently, Yamada and Tanaka with coworkers have developed an original supramolecular phthalocyanine-porphyrin assembly based on μ -nitrido diiron platform for catalytic oxidation of light alkanes (Fig. 15) [69,70].

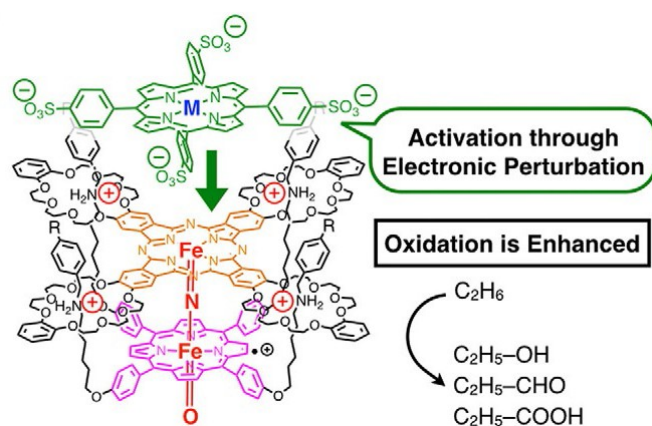


Fig. 15. Schematic representation of supramolecular concept based on μ -nitrido diiron phthalocyanine-porphyrin heteroleptic complexes (Porph)Fe- μ N-Fe(Pc)@MTPPS (M = Cu, Ni). Reproduced with permission from ref. 70. Copyright (2019) John Wiley and Sons.

The μ -nitrido complex was prepared from the metal-free cofacial porphyrin-phthalocyanine heterodimer which structure was stabilized by fourfold rotaxane formation. The iron insertion followed by the treatment with NaN_3 provided the target μ -nitrido complex (Porph)Fe- μ N-Fe(Pc) with a 28 % yield. The sharp signals in ^1H NMR spectrum in 0 - 9 ppm region indicated diamagnetic Fe(IV)Fe(IV) state. According to the Fe K-edge EXAFS spectrum, the Fe- μ N length was 1.72 Å which is longer than those of published regular μ -nitrido diiron complexes (1.65-1.68 Å) [62] owing to steric repulsion of the peripheral organic moieties. Upon incubation of the μ -nitrido dimer with $\text{Cu}^{\text{II}}\text{TPPS}^{4-}$ or $\text{Ni}^{\text{II}}\text{TPPS}^{4-}$ (TPPS $^{4-}$ = 5,10,15,20-tetrakis(4-sulfonatophenyl)porphyrin), the 1:1 supramolecular assemblies were formed according to ESI-TOF mass spectra. Significant broadening and red shift of the Q band of the phthalocyanine fragment as well as a strong higher field shift of the pyrrolic N-H proton (from -2.87 to -11.59 ppm) of the $\text{H}_2\text{TPPS}^{4-}$ confirm the formation of stacked assemblies (Porph)Fe- μ N-Fe(Pc)@CuTPPS and (Porph)Fe- μ N-Fe(Pc)@NiTPPS [69,70].

The (Porph)Fe- μ N-Fe(Pc), (Porph)Fe- μ N-Fe(Pc)@CuTPPS and (Porph)Fe- μ N-Fe(Pc)@NiTPPS were supported onto SiO_2 and their catalytic activities were evaluated in the oxidation of ethane by H_2O_2 in water at 60°C. In line with our previous reports, the oxidation was slow in pure water but in the presence of 51 mM CF_3COOH an efficient oxidation of ethane to $\text{C}_2\text{H}_5\text{OH}$ and CH_3CHO occurred, followed by gradual accumulation of CH_3COOH and HCOOH . The total turnover numbers (TTN) defined as $\text{TTN} = ([\text{C}_2\text{H}_5\text{OH}] + 2[\text{CH}_3\text{CHO}] + 3[\text{CH}_3\text{COOH}] + 6/2[\text{HCOOH}]) / [\text{catalyst}]$ were determined to be 195, 376 and 394 for (Porph)Fe- μ N-Fe(Pc)- SiO_2 , (Porph)Fe- μ N-Fe(Pc)@CuTPPS- SiO_2 and (Porph)Fe- μ N-Fe(Pc)@NiTPPS- SiO_2 , respectively, compared to $\text{TTN} = 289$ for $(\text{FePc}^t\text{Bu}_4)_2\text{N-SiO}_2$ [70]. Importantly, the TTN increased almost lineary over 24 h and bleaching of the supported catalyst was not observed indicating its good stability under reaction conditions. Indeed, the (Porph)Fe- μ N-Fe(Pc)@CuTPPS- SiO_2 catalyst retained ~93 % of its catalytic efficiency after 24 h. When the oxidation of ethane was performed at 100°C using (Porph)Fe- μ N-Fe(Pc)- SiO_2 , the TTN of

1038 was obtained which is comparable with the amount H_2O_2 used (1070 equiv). This implies that over-oxidation of the reactions products to CO_2 was almost negligible.

A distinctive feature of this supramolecular μ -nitrido diiron complex is the Fe(IV)Fe(IV) initial state whereas the previous μ -nitrido diiron phthalocyanine complexes active in the oxidation were in the initial Fe(III)Fe(IV) oxidation state. The putative high-valent diiron oxo species was detected by electrospray-ionization Fourier transform ion cyclotron resonance mass spectrometry (ESI-FT-ICR MS) though the position of oxo group (phthalocyanine or porphyrin site) could not be determined. Yamada, Tanaka and coworkers have proposed a possible mechanism involving both Fe(IV)Fe(IV) and Fe(III)Fe(IV) based catalytic cycles (Fig. 16).

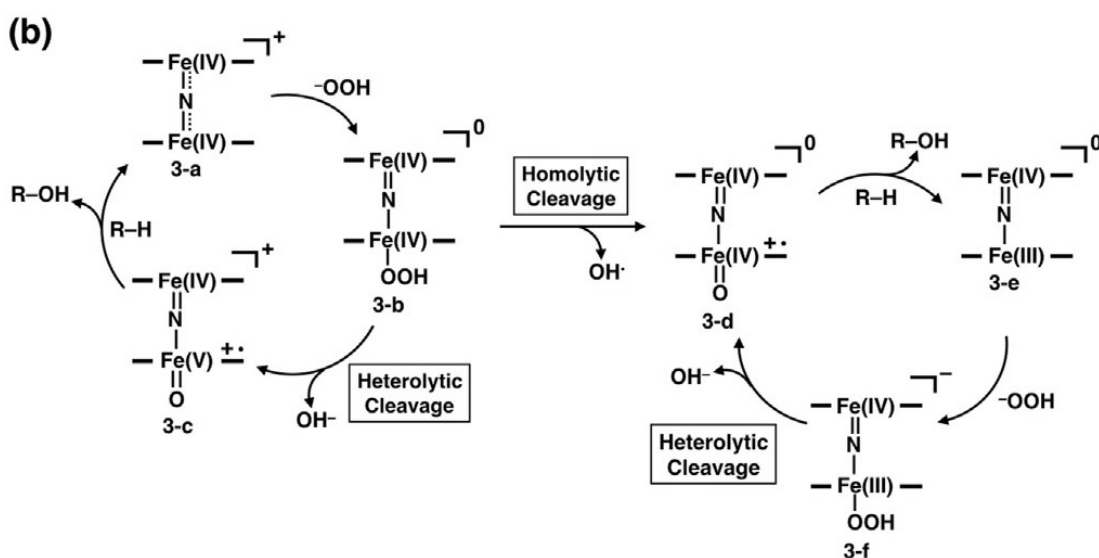


Fig. 16. Proposed reaction mechanism of the oxidation of light alkanes by supramolecular μ -nitrido diiron complex involving Fe(IV)Fe(IV) and Fe(III)Fe(IV) based catalytic cycles. Reproduced with permission from ref. 70. Copyright (2019) John Wiley and Sons.

This, the Fe(IV)Fe(IV) platform seems to be prone to further oxidation. The one-electron oxidation of μ -nitrido diiron (IV) phthalocyanine by peroxide has been reported [71].

The same approach was used for the more challenging oxidation of methane (10 bar) by H_2O_2 in water acidified with CF_3COOH (Fig. 17) [69].

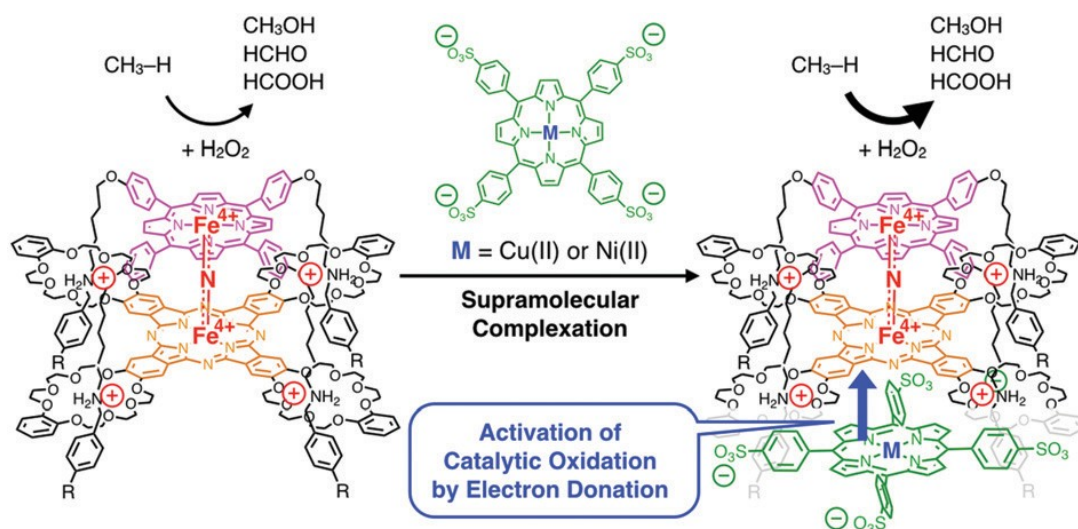


Fig. 17. Supramolecular conjugates for the oxidation of methane. Reproduced from Ref. 69 with permission from the Centre National de la Recherche Scientifique (CNRS) and The Royal Society of Chemistry.

The principal oxidation product was formic acid and the amount of CH₃OH and HCHO were much lower than that of HCOOH even at initial step of the reaction. Again, supramolecular conjugates (Porph)Fe- μ N-Fe(Pc)@CuTPPS-SiO₂ and (Porph)Fe- μ N-Fe(Pc)@NiTPPS-SiO₂ showed superior TTN of 44 and 47, respectively, compared with TTN = 30 obtained with (Porph)Fe- μ N-Fe(Pc)-SiO₂. A superior catalytic activity of the supramolecular conjugates in the oxidation of methane and ethane was proposed to be due to the electronic perturbation through π - π stacking [69]. This elegant work showed a promising strategy for controlling a catalytic activity of μ -nitrido diiron scaffold.

3.3 Oxidation of alkanes

Catalytic properties of μ -nitrido diiron phthalocyanines are affected by the nature of the oxidant. As shown above, when H₂O₂ oxidant is used, the peroxy intermediate (Pc)Fe^{IV}(μ -N)Fe^{III}(Pc)-O-OH undergoes a heterolytic cleavage of O-O bond to generate (Pc)Fe^{IV}(μ -N)Fe^{IV}(Pc⁺)=O. In the case of ^tBuOOH, the initially formed (Pc)Fe^{IV}(μ -N)Fe^{III}(Pc)-O-O^tBu analog is subjected to the

homolytic O-O bond cleavage affording two one-electron oxidizing species (Pc)Fe^{IV}(μ-N)Fe^{IV}(Pc)=O and ^tBuO[•] (Fig. 18) [61].

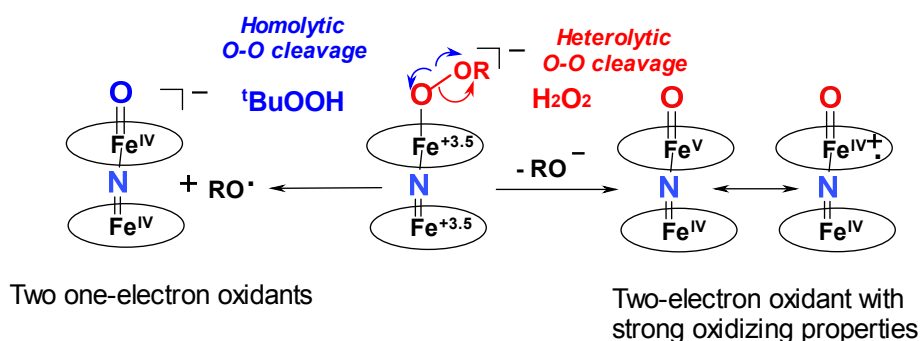


Fig. 18. Formation of μ -nitrido diiron peroxo complexes derived from ^tBuOOH and H₂O₂ and their evolution to different oxo species through homolytic and heterolytic O-O bond cleavages, respectively.

This mechanistic versatility should result in different reactivities depending on the nature of the oxidant used. The reactivity of the (FePc^tBu₄)₂N in combination with ^tBuOOH was studied in the oxidation of alkanes, olefins, aromatic and alkylaromatic compounds [72].

The oxidation of neat cyclohexane by ^tBuOOH (0.2 M) catalyzed by (FePc^tBu₄)₂N (0.1 mM) occurs with the turnover frequency of 3.9 min⁻¹ to provide cyclohexanol (Cy-OH) and cyclohexanone (Cy=O) as principal products in comparable amounts. Along with Cy-OH and Cy=O, bicyclohexyl (Cy-Cy) was formed even in the presence of O₂ and high concentration of ^tBuOOH [72]. This product derived from coupling of cyclohexyl radicals accounted for 8.0% of the reaction products whereas Cy=O and Cy-OH constituted 50.4 and 41.6%, respectively. The formation of Cy-OH and Cy=O in a ~ 1:1 ratio usually takes place when Cy-O-O[•] radicals are formed which interact through Russell mechanism to generate Cy-O-O-O-O-Cy intermediate which, in turn, affords Cy-OH, Cy=O and O₂ upon degradation. The total concentration of products reached 79.2 mM after 6 h and 98.4 mM after 24 h and the total TON achieved 1063 cycles. The product yield on the ^tBuOOH attained 59%. The formation of Cy-Cy implies that considerable amount of cyclohexyl radicals is produced which cannot be totally transformed to

Cy-OH and Cy=O through quenching by oxidizing species. Therefore, the product composition of cyclohexane oxidation by the $(\text{FePc}^t\text{Bu}_4)_2\text{N}-t\text{BuOOH}$ system is consistent with radical oxidation mechanism which involves the $t\text{BuO}^\cdot$ radical and $(\text{Pc})\text{Fe}^{\text{IV}}(\mu\text{-N})\text{Fe}^{\text{IV}}=\text{O}(\text{Pc})$ species generated via the homolytic cleavage of the O-O bond of $(\text{Pc})\text{Fe}^{\text{IV}}(\mu\text{-N})\text{Fe}^{\text{III}}\text{-O-O}^t\text{Bu}(\text{Pc})$.

Significant improvement of the efficiency of cyclohexane oxidation was observed using 0.75 M $t\text{BuOOH}$ added in three portions at 0, 3 and 6 h at 50°C. The portion-wise $t\text{BuOOH}$ addition resulted in higher TON and product yields (Table 1).

Table 1. Oxidation of neat cyclohexane by $(\text{FePc}^t\text{Bu}_4)_2\text{N} - t\text{BuOOH}$ system. Reprinted with permission from ref. 72. Copyright (2017) Elsevier.

Reaction time, h	Concentration, mM			Distribution, % Cy-OH: Cy=O: Cy-Cy	Yield on $t\text{BuOOH}$, % ^b	Total TON
	Cy-OH	Cy=O	Cy-Cy			
3	48.3	59.4	2.2	44 : 54 : 2	68	1099
6	117.8	141.9	5.0	44 : 54 : 2	81	2647
9	195.5	246.5	14.0	43 : 55 : 2	94	4560
23	191.2	323.7	14.7	36 : 61 : 3	114	5296

^a Conditions: 2 mL of cyclohexane (9.26 M), $[(\text{FePc}^t\text{Bu}_4)_2\text{N}] = 0.1$ mM, $t\text{BuOOH}$ was added in three portions at 0, 3 and 6 h, total $[t\text{BuOOH}] = 0.75$ M, 50°C. ^b Yield was based on the amount of the oxidant $t\text{BuOOH}$ added before analysis taking into account that two oxidant equivalents are consumed to produce Cy=O. The yield of 114 % (last line) is due to the involvement of O_2 in the oxidation reaction.

The distribution of reaction products was quite constant during all the course of the reaction. The $(\text{FePc}^t\text{Bu}_4)_2\text{N}$ complex was rather stable under reaction conditions. According to UV-vis analysis of the spent reaction mixture only 10% of the complex was destroyed during reaction. The total TON continuously increased with the reaction time to achieve almost 5300 turnovers. Significantly, the total concentration of Cy=O and Cy-OH attained more than 0.5 M after 23 h. The portion-wise addition of $t\text{BuOOH}$ led to decrease of the Cy-Cy content down to 2-3 %. Of particular interest is the fact that the oxidation of neat cyclohexane provided a 5.9% conversion. The yields of the oxidation products based on the $t\text{BuOOH}$ amount progressively increased from 68% (3 h) to 81% (6 h) and 94% (9 h) to attain 114% after 23 h suggesting the involvement of O_2 in the reaction.

The particular feature of the $(\text{FePc}^t\text{Bu}_4)_2\text{N} - {}^t\text{BuOOH}$ system is the simultaneous production of two active species able to cleave C-H bonds to generate radicals which then recombine forming coupling products or can be intercepted by O_2 to generate peroxy radicals which initiate radical oxidation reaction. (Fig. 19).

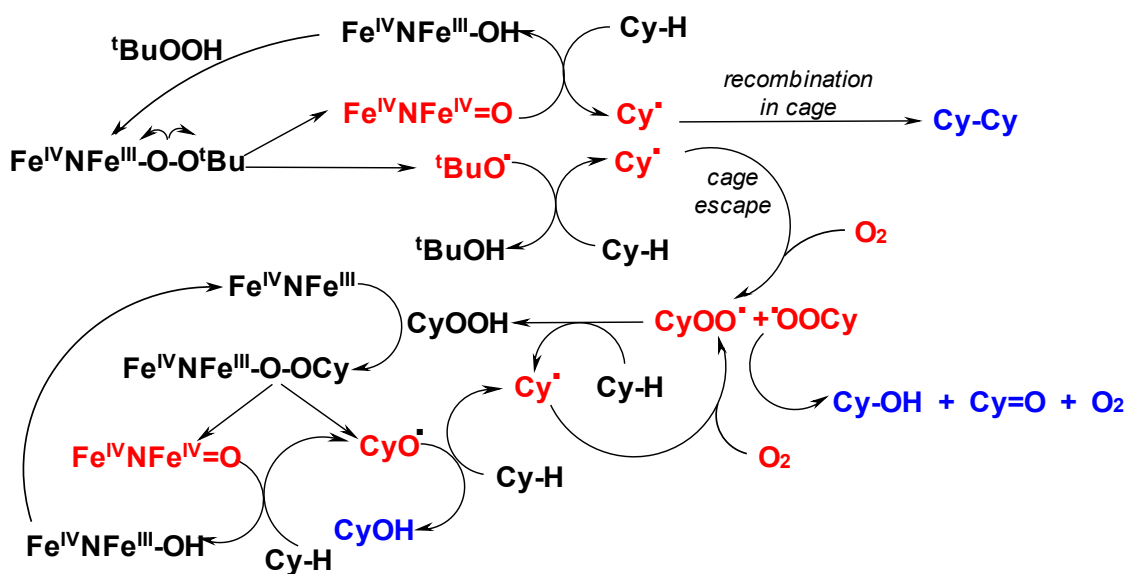


Fig. 19. Proposed mechanism of the oxidation of cyclohexane by $(\text{FePc}^t\text{Bu}_4)_2\text{N} - {}^t\text{BuOOH}$ system. Phthalocyanine ligands are omitted for clarity. Species reacting with C-H bonds are depicted in red and principal products are in blue. Reprinted with permission from ref. 72. Copyright (2017) Elsevier.

Cyclohexyl hydroperoxyde CyOOH , important intermediate product of this radical pathway, can also be activated by $(\text{FePc}^t\text{Bu}_4)_2\text{N}$ to produce $(\text{Pc})\text{Fe}^{\text{IV}}(\mu\text{-N})\text{Fe}^{\text{III}}(\text{Pc})\text{-O-O}^t\text{Cy}$ followed by generation of $(\text{Pc})\text{Fe}^{\text{IV}}(\mu\text{-N})\text{Fe}^{\text{IV}}(\text{Pc})=\text{O}$ and CyO^{\bullet} radical which in turn initiate further oxidation chains. Several lines of evidence demonstrate that the $(\text{FePc}^t\text{Bu}_4)_2\text{N} - {}^t\text{BuOOH}$ system operates via one-electron oxidation pathways involving free radicals [72]. The $(\text{FePc}^t\text{Bu}_4)_2\text{N} - {}^t\text{BuOOH}$ system was also efficient in the oxidation of adamantane, cyclohexane and toluene [72].

Hydrogen peroxide can be also used for the oxidation of alkanes. The oxidation of cyclohexane by $(\text{FePc}^t\text{Bu}_4)_2\text{N} - \text{H}_2\text{O}_2$ system was strongly enhanced in the presence of 10 mM perfluorocarboxylic acids [73]. Acetic and sulfuric acids were less efficient whereas the

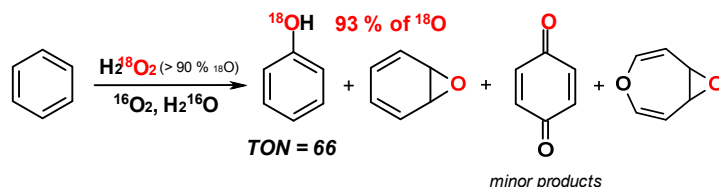
efficiency of perfluorocarboxylic acids in terms of TON depended on the number of carbon atoms:

CF_3COOH (TON = 504) > $\text{CF}_3\text{CF}_2\text{COOH}$ (478) > $\text{CF}_3(\text{CF}_2)_3\text{COOH}$ (353) > $\text{CF}_3(\text{CF}_2)_6\text{COOH}$ (290) ~ $\text{CF}_3(\text{CF}_2)_8\text{COOH}$ (311) > $\text{CF}_3(\text{CF}_2)_{10}\text{COOH}$ (92) >> no acid (32)

Evaluation of Al_2O_3 , Fe_2O_3 , SiO_2 , and ZrO_2 supports showed that the $(\text{FePc}^t\text{Bu}_4)_2\text{N-Al}_2\text{O}_3$ catalyst exhibited the highest activity of 109 turnover numbers without any acid additive [74]. The strong acidic sites of Al_2O_3 support were proposed to be responsible for this enhanced catalytic activity.

3.4 Oxidation of benzene: evidence for biomimetic reactivity

The oxidation of benzene is an important industrial process and hydroxylation of aromatic C-H bonds is related to essential biological functions. Several enzymes including cytochromes P-450 perform the hydroxylation of aromatic compounds through high-valent iron oxo species. The principal mechanisms of enzymatic oxidation of benzene were considered by de Visser and Shaik [75]. Characteristic features of the biological hydroxylation of arenes are (i) intermediate formation of arene epoxide and (ii) substituent migration from the hydroxylation site to the adjacent position (NIH shift). Bio-inspired complexes capable of efficiently oxidizing benzene are still rare [76]. The oxidation of benzene by $(\text{FePc}^t\text{Bu}_4)_2\text{N-H}_2\text{O}_2$ afforded phenol as the principal product (TON = 66) as well as smaller amounts of benzene epoxide, *sym*-oxepin oxide and benzoquinone (Fig. 20) [53].



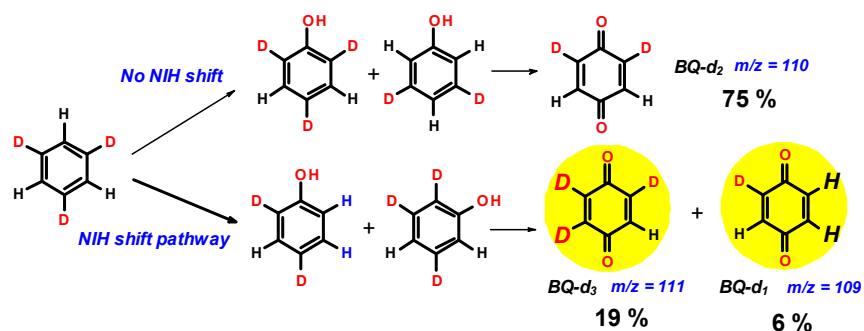


Fig. 20. Mechanistic features of oxidation of benzene catalyzed by (FePc^tBu₄)₂N : incorporation of ¹⁸O from H₂¹⁸O₂, formation of benzene epoxide and detection of NIH shift. Reprinted with permission from ref. 60. Copyright (2016) American Chemical Society.

The formation of benzene epoxide and *sym*-oxepin oxide is mechanistically important. Benzene epoxide is assumed to be in rapid equilibrium with tautomeric oxepin [77] which can be also epoxidized to *sym*-oxepin oxide by P-450 monooxygenase [78]. Thus, the (FePc^tBu₄)₂N-H₂O₂ system oxidizes benzene to benzene epoxide in the first step followed by its isomerization to phenol. The formation of notable amount of *sym*-oxepin oxide via the epoxidation of oxepin, tautomeric form of benzene epoxide, strongly suggests that the oxidation route through the PhH epoxidation should be principal one.

Intermolecular and intramolecular kinetic isotope effects (k_H/k_D) on phenol formation in the competitive oxidation of a 1:1 C₆H₆ /C₆D₆ mixture and using benzene-1,3,5-*d*₃ were determined at 25°C to be 1.21±0.04 and 1.29±0.03, respectively. These k_H/k_D values are not consistent with the formation of σ -complex since in this case the inverse k_H/k_D (<1) are expected [75]. A labelling study using H₂¹⁸O₂ as the oxidant in the presence of unlabeled ¹⁶O₂ and H₂¹⁶O revealed the exclusive incorporation of ¹⁸O from H₂¹⁸O₂ to provide Ph¹⁸OH [53].

The enzymatic formation of arene epoxides is accompanied by the NIH shift when high-valent iron oxo species are involved. In order to examine a possible NIH shift, we have introduced 1,3,5-trideuterobenzene as a mechanistic probe [53]. On the basis of the isotopic composition of 1,4-benzoquinone obtained by the further oxidation of phenol one can conclude

whether the NIH shift occurs (Fig. 20). If there is no NIH shift, two isotopomeric phenols should be obtained affording the only quinone-d₂ via further oxidation. In the alternative scenario, initially formed benzene epoxide undergoes to H/D shift resulting in two 2,4-cyclohexadien-1-ones which enolization leads to four phenols including NIH-shifted ones with two adjacent D- or H-atoms. Along with quinone-d₂, their oxidation provides quinone-d₁ and quinone-d₃ which can only be obtained according to this mechanism. Analysis of the isotopic composition of 1,4-benzoquinone produced in the oxidation of benzene by (FePc^tBu₄)₂N-H₂O₂ system has shown 19% quinone-d₁ and 6% of quinone-d₃ that evidences the NIH-shift. Therefore, exclusive incorporation of the H₂¹⁸O₂ oxygen to phenol, formation of benzene epoxide and NIH shift observed in the benzene oxidation by (FePc^tBu₄)₂N-H₂O₂ system are similar to mechanistic features of biological oxidation. These results further confirms the involvement of high-valent diiron oxo-species in the oxidation reactions catalyzed by μ-nitrido diiron complexes.

3.5. Oxidative dehalogenation and defluorination

The incubation of (FePc^tBu₄)₂N with ^tBuOOH in CH₂Cl₂ or CH₂Br₂ solvents resulted in their dehalogenation to form stable Cl-(Pc)Fe^{IV}(μ-N)Fe^{IV}(Pc⁺)-Cl and Br-(Pc)Fe^{IV}(μ-N)Fe^{IV}(Pc⁺)-Br complexes with high isolated yields [54]. The formation of Cl-(Pc)Fe^{IV}(μ-N)Fe^{IV}(Pc⁺)-Cl implies the cleavage of the C-Cl bond in CH₂Cl₂ widely used as the solvent for the oxidation reactions. The strong and narrow EPR signal at g = 2.0012 (11 G width) due to the cation-radical of phthalocyanine and one doublet signal in Mössbauer spectrum with δ = - 0.10 mm.s⁻¹ and ΔE_{Q1} = 1.64 mm.s⁻¹ due to identical Fe(IV) sites imply structures isoelectronic to high-valent oxo iron species relevant to biological and biomimetic oxidations. The Fe(IV) state was confirmed by intensive pre-edge energy peaks in XANES spectra at 7115.2 eV with typical for such a manifold the second lobe at 7113.4 eV. The Fe K-edge EXAFS analysis of X-(Pc)Fe^{IV}(μ-N)Fe^{IV}(Pc⁺)-X showed a symmetric Fe-N-Fe fragment with a 3.39 Å Fe-Fe distance and the Fe-Cl and Fe-Br bond lengths of 2.33 and 2.54 Å, respectively [54].

Can this reactivity be extended to fluorinated compounds? Catalytic transformation of C-F bonds, the strongest organic single bonds, has been a long-standing challenge in chemistry for both fundamental and practical reasons. Fluorinated organic compounds are increasingly used in many applications due to unique properties of C-F bonds (high thermal and oxidative stability, C-F bond strength, low polarity, weak intermolecular interactions). Carbon-fluorine bonds have a pivotal role in pharmaceuticals, agrochemicals, materials (liquid crystals, polymers, solvents, tracers for positron emission tomography, etc.). For instance, 40 % of agrochemicals and 25 % of pharmaceuticals currently used contain C-F bonds. Although a variety of efficient systems for C-F activation based on electron-rich organometallic complexes, reduction and nucleophilic substitution reactions have been developed, the oxidative transformations of poly- and especially perfluorinated compounds are practically unknown in chemistry and biology. Moreover, since fluorine is the most electronegative element, the reaction of heavily fluorinated compounds with strong oxidants (highly electron-deficient species) has been considered as almost impossible.

Inspired by unusual oxidative dechlorination of CH_2Cl_2 , we screened the reactivity of $(\text{FePc}^t\text{Bu}_4)_2\text{N}$ toward different halogenated compounds. Remarkably, the oxidative dehalogenation can be extended to fluorinated aromatics including C_6F_6 with $\text{BDE}_{\text{C-F}}=154 \text{ kcal mol}^{-1}$. Treatment of $(\text{FePc}^t\text{Bu}_4)_2\text{N}$ with 30 equiv. $^t\text{BuOOH}$ in $\text{C}_6\text{F}_6/\text{C}_6\text{H}_6$ mixture at 60°C for 6 h resulted in the formation of the complex $[(\text{Pc})\text{F}-\text{Fe}^{\text{IV}}(\mu\text{-N})\text{Fe}^{\text{IV}}-\text{F}(\text{Pc}^+)]$ with 80 % isolated yield which was stable under reaction conditions (Fig. 21) [59].

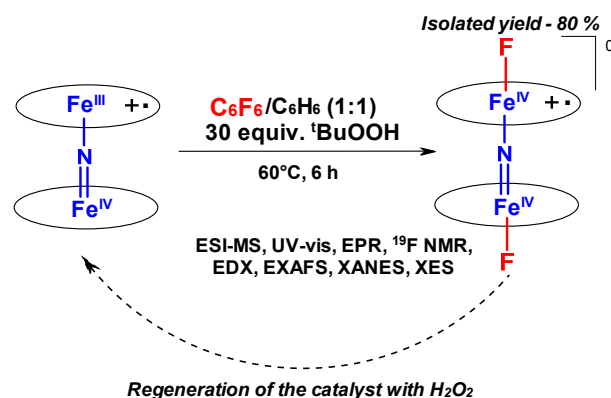
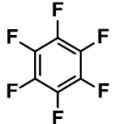
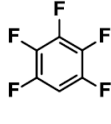
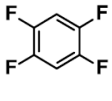
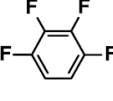
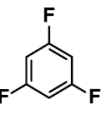
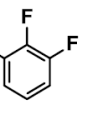
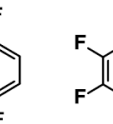
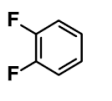


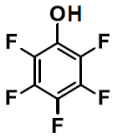
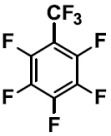
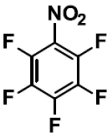
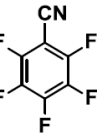
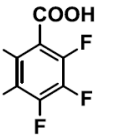
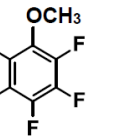
Fig. 21. Stoichiometric formation of [(Pc)(F)Fe^{IV}(μ-N)Fe^{IV}(F)(Pc⁺)] and regeneration of the starting complex in the presence of H₂O₂. Adapted with permission from ref. 60. Copyright (2016) American Chemical Society.

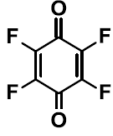
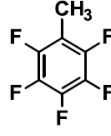
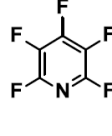
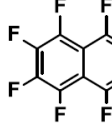
This intermediate involved in stoichiometric defluorination was characterized by ESI-MS, UV-vis, EPR, ¹⁹F NMR, EDX, EXAFS, XANES and XES techniques.

To convert this stoichiometric chemistry to catalytic defluorination reaction, (FePc^tBu₄)₂N should be regenerated by reduction of [(Pc)F-Fe^{IV}(μ-N)Fe^{IV}-F(Pc⁺)]. Spectrophotometric titration of [(Pc)F-Fe^{IV}(μ-N)Fe^{IV}-F(Pc⁺)] by H₂O₂ led to the formation of (FePc^tBu₄)₂N. Thus, H₂O₂ reacts (i) as the oxidant to generate high-valent diiron oxo species capable of defluorinating of perfluorinated aromatics; and (ii) as reductant of [(Pc)F-Fe^{IV}(μ-N)Fe^{IV}-F(Pc⁺)] to the catalyst resting state to complete the catalytic cycle. The homogeneous (FePc^tBu₄)₂N-H₂O₂ system efficiently converts a range of aromatic compounds with various fluorination pattern including perfluorinated and polyfluorinated compounds bearing different functional groups with high TON (Fig. 22) [59].

Homogeneous defluorination reactions in CD₃CN

								
Conversion (TON)								
(FePc) ₂ N - H ₂ O ₂	29 % (226)	33 % (152)	59 % (341)	41 % (336)	66 % (351)	41 % (169)	69 % (240)	47 % (120)
Fenton system	0 %	n.d.	0 %	0 %	n.d.	n.d.	0 %	0 %

						
Conversion (TON)						
(FePc) ₂ N - H ₂ O ₂	82 % (818)	30 % (242)	45 % (376)	20 % (141)	31 % (178)	40 % (188)
Fenton system	7 % (45)	<2 % (<15)	<2 % (<15)	<4 % (<9)	<9 % (70)	<3 % (<17)

				
Conversion (TON)				
(FePc) ₂ N - H ₂ O ₂	99 % (986)	45 % (282)	15 % (69)	29 % (150)
Fenton system	98 % (750)	<7 % (43)	<2 % (<17)	11 % (78)

Heterogeneous defluorination reactions with supported catalyst in D₂O

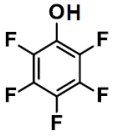

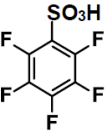
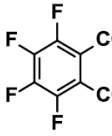
				
Conversion (TON)				
(FePc) ₂ N - H ₂ O ₂	98 % (4825)	76 % (2950)	53 % (2140)	56 % (1730)

Fig. 22. Catalytic defluorination of poly- and perfluorinated aromatics by (FePc^tBu₄)₂N-H₂O₂. Conditions: catalyst:substrate:oxidant=1:250:4000, 60°C, 15 h. Homogeneous and heterogeneous reactions using carbon-supported catalyst were performed in CD₃CN and D₂O, respectively. TONs were calculated as moles of F⁻ per mole of catalyst.

Remarkably, (FePc^tBu₄)₂N mediates defluorination of C₆F₆ converting 3.12 from 6 fluorine atoms to F⁻ whereas the oxidative metabolism for perfluorinated species *via* enzymatic pathways including cytochrome P450 is unknown. In marked contrast to usual organometallic and reductive approaches to C-F bond activation which need the rigorous inert and anhydrous conditions, the (FePc^tBu₄)₂N-H₂O₂ system shows a high defluorination efficiency in water (Fig. 22). Moreover, the defluorination activity in water using supported catalyst was much higher

compared to that obtained in MeCN (Fig. 22). Thus, when pentafluorophenol was used as the substrate, 4825 C-F bonds per catalyst molecule were cleaved with release of fluoride anion.

Taking into account that poly- and perhalogenated aromatic compounds are recalcitrant contaminants and fluorinated compounds are extremely persistent in the environment owing to their very slow biodegradation, the development of practical disposal methods for these emerging pollutants is of vital importance. In this context, the supported $(\text{FePc}^t\text{Bu}_4)_2\text{N}-\text{H}_2\text{O}_2$ system operating in water appears to be particularly suitable. To confirm the practical aspect of this oxidative approach, we have studied in details the transformation of pentafluorophenol. Quantitative analysis of the reaction products by GC-MS, ^{19}F NMR and total carbon determination showed the formation of hydrofluoric acid and CO_2/CO resulting in 89 % defluorination and 54 % organic carbon loss (Fig. 23).

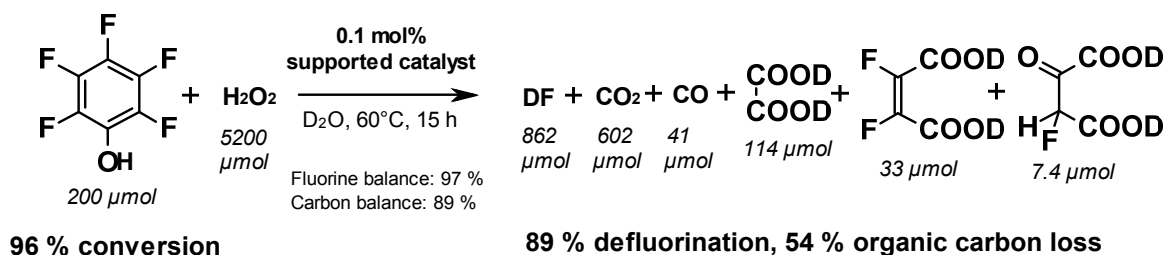


Fig. 23. Catalytic mineralization of pentafluorophenol in water using supported onto carbon $(\text{FePc}^t\text{Bu}_4)_2\text{N}$.

μ -Nitrido diiron complexes also showed promising results in the degradation of chlorinated phenols [79]. Homogeneous aqueous oxidation of 2,6-dichlorophenol and 2,4,6-trichlorophenol by H_2O_2 was efficiently catalyzed by water-soluble μ -nitrido diiron tetrasulfophthalocyanine $(\text{FePcS})_2\text{N}$. The same catalytic system was successfully applied for example for the degradation of toxic Orange II reagent in water [80]. Therefore, this oxidative approach to the degradation of recalcitrant pollutants seems to be particularly suitable from practical point of view. Indeed, (i) earth abundant and non-toxic iron-based catalyst is available on a large scale and industrially relevant; (ii) the μ -nitrido diiron catalyst can be readily

immobilized onto different supports; (iii) environmentally compatible H₂O₂ oxidant is industrially available; (iv) the catalytic system is tolerant to water and air and shows a large substrate scope; (v) the process can be carried out in concentrated organic solutions (e.g. for the treatment of industrial wastes) or in water including diluted solutions (for treatment of contaminated water). For all these reasons we believe that this novel approach might be useful for the development of novel remediation processes.

The uncommon defluorination of aromatic compounds via oxidation pathway raises questions on the mechanistic background of this striking reactivity. How does the extremely electron-deficient (Pc)Fe^{IV}(μ-N)Fe^{IV}(Pc⁺)=O species react with the C-F bond formed by the most electronegative element? Following mechanistic scenarios have been evaluated: (A) free-radical Fenton oxidation; (B) electrophilic attack; (C) nucleophilic substitution and (D) initial epoxidation of aromatic cycle.

(A) Benzenes with different fluorination pattern were totally stable under Fenton conditions (Fig. 22) [59,81]. The substrates having functional groups exhibited conversions at the detection limit. These results are not in agreement with involvement of OH[•] radicals.

(B) 1,3,5-trichloro-2,4,6-trifluorobenzene afforded phenols obtained preferentially *via* F rather than Cl elimination (97:3 ratio). The oxidation of 1,3,5-trifluorobenzene also led to phenol issued principally from F elimination rather than from the C-H oxidation (98:2 ratio) (Fig. 24).

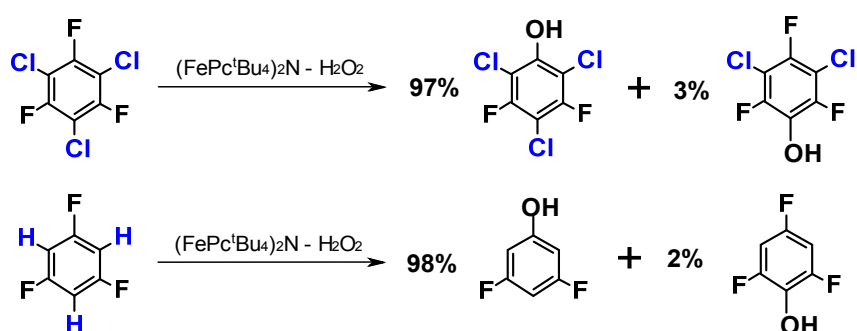


Fig. 24. Comparison of reactivity of aromatic C-F, C-Cl and C-H bonds exhibited by (FePc^tBu₄)₂N-H₂O₂ system.

Despite the strong electrophilic properties of ultra high-valent diiron oxo species, the reactivity of aromatic C-F vs C-Cl and C-H bonds observed in intramolecular competition using C₆F₃Cl₃ and C₆F₃H₃ probes is not compatible with electrophilic attack of oxo species on the C-X bond.

(C) The conversions of fluorinated benzenes decrease with the increase of the number of fluorine groups (Fig. 22). Other reactivity trends also disfavor this mechanism [59].

(D) Oxidation of aromatic compounds including halogenated benzenes by cytochrome P450 Compound I involves the formation of arene epoxides and NIH shift [75]. Similarly, the (FePc^tBu₄)₂N mediates the oxidation of benzene *via* benzene epoxide accompanied by NIH shift [53]. Thus, the initial epoxidation of fluoroarene can be considered as plausible route. Although identification of fluoroarene epoxides is hampered by low ESI-MS response and their low stability at GC-MS conditions, we could detect an epoxide in the oxidation of perfluoro-naphthalene. Using 1,4-difluorobenzene probe allowed detecting the very rare fluorinated NIH shift to confirm the epoxidation pathway as initial step of defluorination reaction [59].

To get deeper insight into this unusual reactivity, detailed DFT analysis of the mechanism of defluorination of hexafluorobenzene by μ -nitrido diiron oxo species were carried out [82]. According to calculations, the reaction proceeds via a rate-determining aromatic addition of diiron oxo species followed by 1,2-fluoride shift to form the ketone intermediate, which can further rearrange to the phenol (Fig. 25).

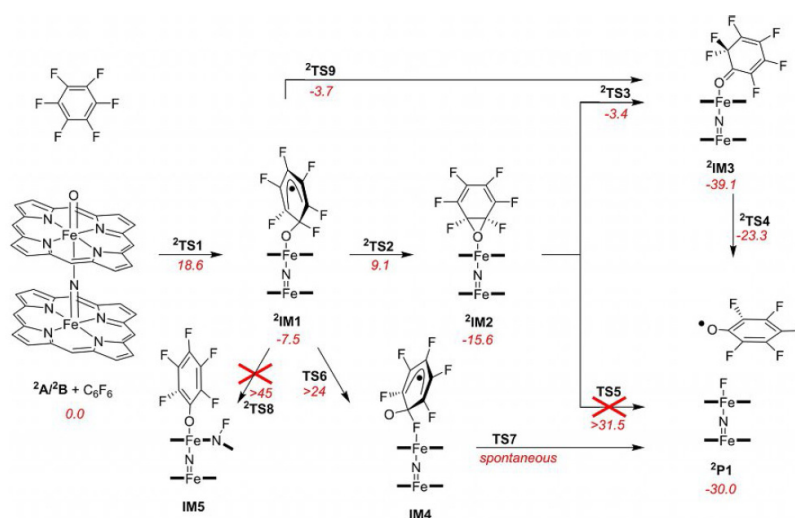


Fig. 25. Mechanism of defluorination reaction explored by DFT calculations. Energy values are in kcal mol⁻¹. Reproduced with permission from ref. 82. Copyright (2019) John Wiley and Sons.

The defluorination of perfluorinated aromatics via oxidative pathway proceeds through a completely different mechanism in comparison to that of aromatic C-H hydroxylation by mononuclear high-valent iron oxo species such as Compound I of cytochrome P450 [82].

4. Evolution of binuclear platform

4.1. μ -Oxo complexes

The progress in the preparation, characterization and applications of μ -oxo dimeric complexes with various metals and macrocyclic ligands has been recently reviewed [83]. It is of interest to study the role of the single-atom bridging group. To this aim, the structural and electronic properties of the three diiron octapropylporphyrazine complexes (FePzPr₈)₂X (X = C, N, O) with Fe(III)- μ O-Fe(III), Fe(III)- μ N-(Fe(IV)) and Fe(IV)- μ C-Fe(IV) were investigated in details in recent comparative studies (see Fig. 26 for their structures) [84,85].

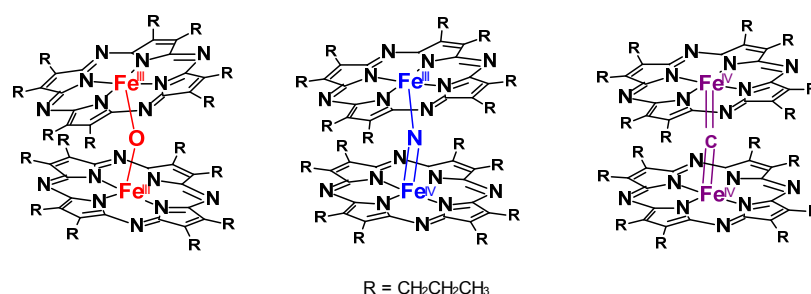


Fig. 26. Structures of μ -oxo, μ -nitrido and μ -carbido diiron octapropylporphyrazines complexes.

Mössbauer study and DFT calculations indicated the increase of covalency of Fe-X bond in the μ -oxo \rightarrow μ -nitrido \rightarrow μ -carbido row and their low-spin character, a singlet state for μ -oxo and μ -carbido and a doublet state for μ -nitrido [85]. These complexes catalyze cyclopropanation of styrene and its derivatives with 0.1 mol% loading and 1.2 equiv ethyl diazoacetate (EDA). The μ -oxo diiron complex was shown to be the most efficient to afford 95-100 % and 82-100 %

cyclopropanation yields in case of styrenes bearing electron-donating and electron-withdrawing substituents, respectively (Table 2).

Table 2. Catalytic cyclopropanation of aromatic and aliphatic olefins by EDA catalyzed by (FePzPr₈)₂O. Reprinted with permission from ref. 85. Copyright (2020) American Chemical Society.

Entry	Substrate	Cyclopropanation		EDA dimerization,
		Yield, ^a %	<i>trans/cis</i> ratio	Yield of <i>cis/trans</i> , ^b %
1	4-methoxystyrene	100	76:24	6/0
2	4-methylstyrene	100	77:23	6/0
3	3-methylstyrene	99	76:24	8/<1
4	4-fluorostyrene	82	73:27	17/1
5	4-cyanostyrene	100	68:32	9/<1
6	pentafluorostyrene	89	80:20	11/1
7	α -methylstyrene	100	63:37	7/<1
8	1,1-diphenylethylene	100	-	5/<1
9	cyclohexene	0	-	76/3
10	<i>n</i> -butylvinylether	58	55:45	19/1
11	2,3-dimethyl-1,3-butadiene ^c	66	71:29	12/<1

^a Yields of cyclopropanation products are based on the initial amount of olefin. ^b Yields of EDA dimerization products are based on the initial amount of EDA. ^c Yield of the products of double cyclopropanation was 33 %.

The carbene transfer ability is usually attributed to metal carbene species [4]. While mononuclear porphyrinoid complexes have been extensively investigated for carbene transfer reactions, their binuclear counterparts have not yet been explored as catalysts for these rapidly developing field. To gain insight into possible participation of binuclear diiron carbene species and to understand the influence of the electronic structure on reactivity, we have performed a

detailed DFT study of the model three diiron porpyrazine complexes having no propyl groups and bearing carbene ligands. μ -O and μ -N carbene complexes show significant spin density at carbon atom of carbene (0.9 e spin density) and therefore can be regarded as radicaloid species. While μ -nitrido and μ -carbido carbene complexes have LUMOs localized on π^* orbitals of the distal Pz ligand, LUMO of the μ -O species is the unoccupied β 2p_y orbital of the radical carbon atom of carbene species (Fig. 27) [85].

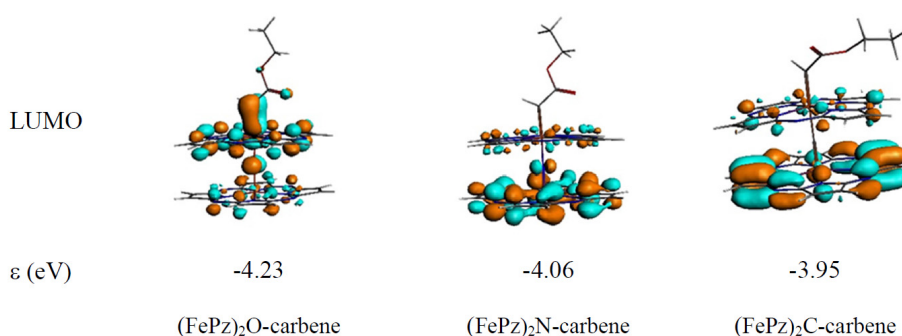


Fig. 27. LUMO of the three (FePz)₂X-carbene species calculated with B3LYP/TZ2P, eigenvalues in eV. Reprinted with permission from ref. 85. Copyright (2020) American Chemical Society.

This difference in electronic structures can explain the superior activity of μ -O-based species and lower reactivity of μ -C and μ -N entities. The former structure should favor the initial radical addition to double bond of styrene followed by cyclization leading to cyclopropane ring. Recent DFT calculations showed that iron mononuclear porphyrinoid carbene species can adapt different electronic configurations that should determine their reactivity [86]. In this connection, their binuclear counterparts can provide even a larger range of the structural and electronic configurations and novel reactivity patterns and reaction landscapes can be probably discovered.

Tetracarbene macrocyclic iron complexes recently introduced as potential catalysts for oxidation can also form μ -oxo dimeric species (Fig. 28) [87].

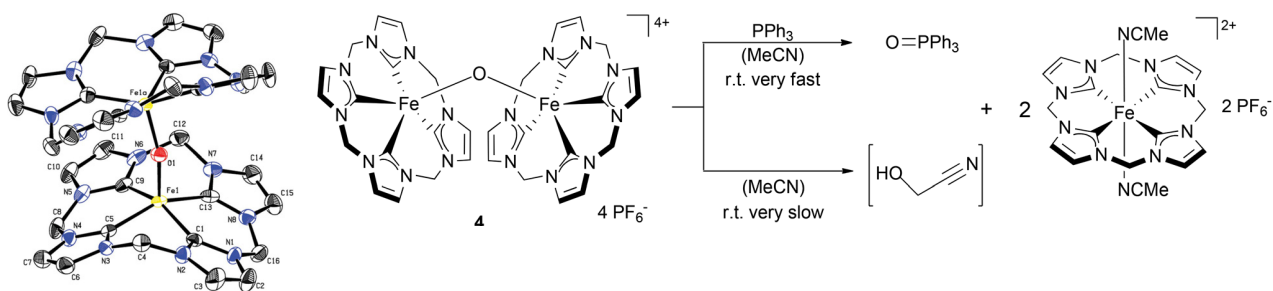


Fig. 28. Crystal structure of μ -oxo diiron complex supported by N-heterocyclic tetracarbene ligand which shows sluggish oxidizing properties. Ref. 27. Published by The Royal Society of Chemistry.

The structure shows a distorted square pyramidal geometry with N-heterocyclic tetracarbene ligands (NHC) coordinated in saddle distorted mode with Fe-O distance of 1.732 Å and the Fe-O-Fe angle of 162.7°. Noteworthy, the μ -oxo diiron(III) species is capable of oxidizing PPh₃ and even CH₃CN though the latter reaction is very slow. Related μ -oxo diiron complex supported by another NHC ligand selectively oxidized dihydroanthracene to anthracene [88].

Two porphyrinoid macrocycles of μ -oxo dimer can be connected by different linkers [89-95]. Several such constructions with rigid and flexible linkers were prepared and structurally characterized (Fig. 29) [96].

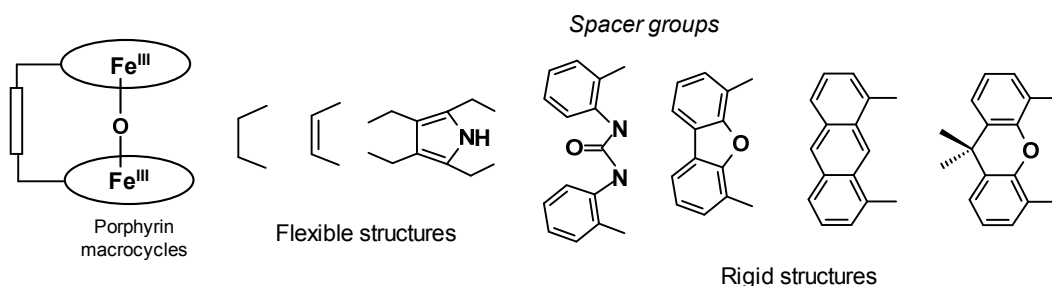


Fig. 29. Structurally characterized μ -oxo diiron complexes with linked porphyrin ligands. Reprinted with permission from ref. 83. Copyright (2019) Elsevier.

The chemistry of these complexes, structural and spectroscopic properties were described in details in the recent review by Rath and co-workers [96]. Herein we briefly discuss the most important properties of these diiron(III) high-spin ($S = 5/2$) systems and further detailed information can be found in ref. 96. The dimeric constructions with ethane, ethene and pyrrole

linkers are quite flexible. The switching between closed and open conformations is triggered by the addition of base or acid resulting in the distinctive colour changes. X-ray structures of the μ -oxo complexes show cofacial arrangement of distorted porphyrin macrocycles with bent Fe-O-Fe fragments: 147.9, 150.9 and 151.97° for ethane, ethene and pyrrole linked complexes, respectively. More rigid aromatic spacers of covalently linked μ -oxo complexes provide less bent structures with Fe-O-Fe angles of 165.7 – 174.8° and longer Fe-Fe distances (3.491-3.511 Å vs 3.409-3.454 Å) and mean plane separations (up to 4.74 Å vs 4.33 Å) [96]. Two Fe^{III} centers in the flexible ethane- and pyrrole-linked μ -oxo species are strongly antiferromagnetically coupled: $J = -126.6 \text{ cm}^{-1}$ [91] and $J = -137.7 \text{ cm}^{-1}$ [89], respectively. Therefore, tuning of the structure of μ -oxo diiron fragment permits a fine control of the interaction and electronic communication between porphyrin moieties of dimer. Furthermore, μ -oxo dimers bearing other porphyrinoid ligands, e.g. oxoporphyrin, azaporphyrin, porphyrazine, corrole, porphodimethene, dioxoporphodimethene, chlorine, were prepared [96]. Consequently, the properties of μ -oxo dimeric species can be also tuned by the appropriate choice of supporting porphyrin-like ligand. Such μ -oxo bimetallic Pacman constructions have been used for photochemical generation of high-valent oxo species via disproportionation of the M-O-M unit and utilization of dioxygen without sacrificial reductants in clean oxidation reactions (Fig. 30) [97].

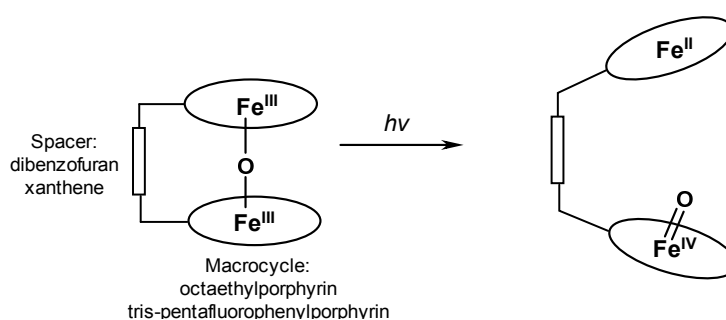


Fig. 30. Photogeneration of iron oxo species from iron Pacman porphyrins. Reprinted with permission from ref. 83. Copyright (2019) Elsevier.

4.2. μ -hydroxo complexes

The protonation of covalently linked μ -oxo diiron porphyrin constructions by strong acids with weakly coordinated anions (e.g. ClO_4^- , PF_6^- , SbF_6^- , BF_4^-) resulted in corresponding μ -hydroxo

species [89,96,98]. The protonation makes the Fe-OH-Fe angle more bent and two porphyrin moieties become closer to each other. Their increased interaction results in unequally distorted porphyrin cores with two different iron spin states in the μ -hydroxo dimer molecule as evidenced by Mössbauer studies [99]. The nature and size of anion influence the iron spin state via the interaction with OH group and iron centers. The calculations showed that the subtle environmental perturbations can affect the spin state of iron atoms [91]. The protonation of μ -oxo bridge of pyrrole-linked dimer led to decrease of coupling constants to $J = -42.2 \text{ cm}^{-1}$ (with HBF_4), $J = -42.4 \text{ cm}^{-1}$ (with HPF_6) and $J = -44.1 \text{ cm}^{-1}$ (with HSbF_6) [89]. The lengthening of the Fe-O bond was suggested to be the important factor for the decrease of coupling. On the other hand, ethane-bridged μ -hydroxo dimanganese octaethylporphyrin has two equivalent high-spin Mn(III) sites [90]. Interestingly, molecules of organic solvents, e.g., H_2O , C_6H_6 , PhMe, THF, etc. can be accommodated in the cavity between porphyrin planes [96].

4.3 μ -carbido diiron complexes

The μ -carbido diiron(IV,IV) porphyrin-like complexes are rare stable species containing two iron sites in such a high oxidation state. Their chemistry and spectroscopic characterization have been reviewed by Ercolani and coworkers in 2003 [49]. In recent years, after extensive development of the catalytic chemistry of μ -nitrido diiron phthalocyanines and related complexes [60,61], the interest to the μ -carbido counterparts has been renewed. Despite their high oxidation states, μ -carbido diiron(IV,IV) porphyrinoid complexes were shown to be capable of reacting with peroxides to generate Fe(IV)Fe(IV) porphyrinoid cation-radical intermediates [100-102]. These high-valent species were proposed to be involved in the oxidation of 3,5,7,2',4'-pentahydroxyflavone [103], lycopene [104] and β -carotene [105,106].

4.4 μ -carbido diruthenium complexes

The chemistry of μ -carbido diruthenium porphyrin-like complexes has been less documented [107]. Recently, the synthetic protocols to μ -carbido diruthenium(IV) phthalocyanine complexes have been developed and optimized [108,109]. A series of substituted complexes $(\text{Pc}^*\text{Ru})_2(\mu\text{-C})$

with Pc* = tetra-*tert*-butyl, octa-*n*-butoxy-, tetra-15-crown-5- and hexa-*n*-butoxy-mono-(15-crown-5)-substituted ligands were prepared by two approaches (Fig. 31).

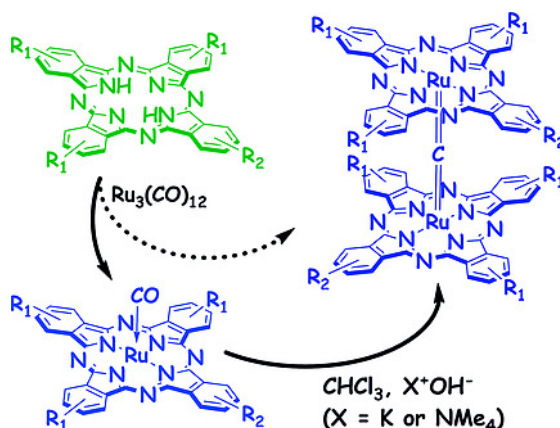


Fig. 31. Two synthetic strategies for the synthesis of μ -carbido diruthenium phthalocyanine complexes. Reprinted with permission from ref. 109. Copyright (2019) Wiley and Sons.

Direct metalation of phthalocyanines with Ru₃(CO)₁₂ in refluxing *o*-dichlorobenzene unexpectedly led to the formation of (Pc*₂Ru)₂(μ -C) along with expected monomeric complexes [Pc*₂Ru](CO). Alternatively, (Pc*₂Ru)₂(μ -C) complexes were obtained by the treatment of [Pc*₂Ru](CO) with chloroform and bases (KOH or NMe₄OH) through dichlorocarbene generated *in situ*, which furnished target complexes in high yields.

The first catalytic applications of μ -carbido diruthenium(IV,IV) phthalocyanine were demonstrated in the carbene insertion into the N-H bonds of aromatic and aliphatic amines and in cyclopropanation of olefins with TON of 580-1000 and 680-1000, respectively (Fig. 32).

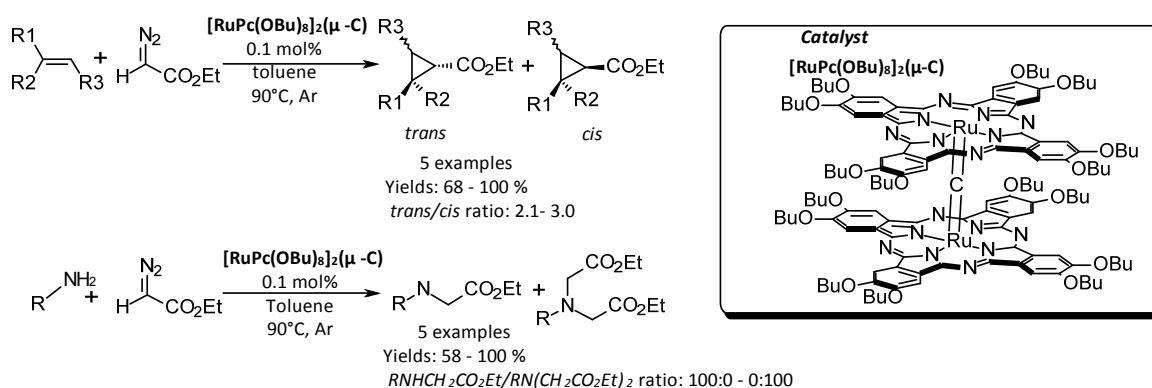


Fig. 32. Carbene transfer reactions from EDA to olefins and amines, catalyzed by $[\text{RuPc}(\text{OBu})_8]_2\text{C}$.

Importantly, 1.2 equiv EDA was used per 1 equiv of substrates and up to quantitative yields of the reaction products were obtained [108]. Even very electron-deficient $\text{C}_6\text{F}_5\text{CH}=\text{CH}_2$ was cyclopropanated with 68 % yield. Furthermore, the carbene insertion to amine N-H bonds was efficient with low catalyst loading and high amine concentration. It is of note, that many metal complexes coordinate the amine substrates that prevent catalytic carbene transfer since complexes without accessible coordination position cannot efficiently activate the carbene precursor. To circumvent this limitation, high catalyst loading and relatively low amine concentrations are usually used resulting in low TON. The $[\text{RuPc}(\text{OBu})_8]_2\text{C}$ does not suffer from this and low catalytic loading can be applied to provide TON up to 1000 [108].

4.5. Tetracarbenic complexes with $\mu\text{-P}$ and $\mu\text{-S}_2$ bridges

Meyer, Ye and coworkers have recently prepared the first macrocyclic tetracarbene complex with two iron sites connected by $\mu\text{-phosphido}$ bridge using sodium phosphoethynolate $\text{Na}(\text{PCO})$ as a synthon for P transferring (Fig. 33) [110].

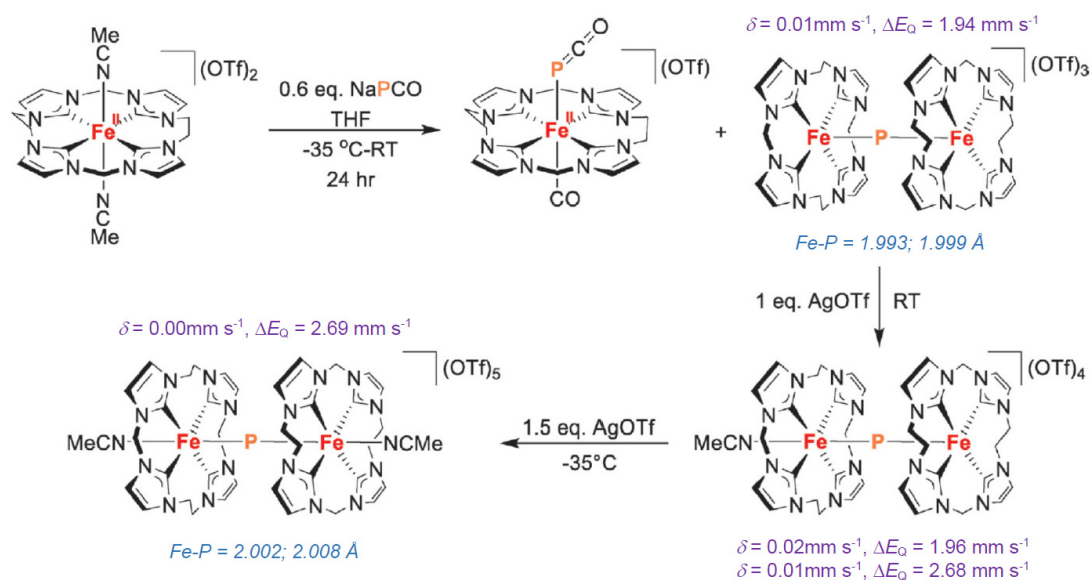


Fig. 33. Preparation of $\mu\text{-phosphido}$ diiron macrocyclic tetracarbene complex in Fe(III)Fe(III), Fe(III)Fe(IV) and Fe(IV)Fe(IV) oxidation states. Adapted with permission from ref. 110. Copyright (2019) Wiley and Sons.

This unprecedented complex contains a linear Fe-(μ P)-Fe motif (178.3° angle) with a “naked” bridged phosphorus which shows +1480 ppm signal in the ^{31}P NMR spectrum. Importantly, this binuclear complex features three stable oxidation states, Fe(III)Fe(III), Fe(III)Fe(IV) and Fe(IV)Fe(IV), all of them have been isolated and fully characterized by X-ray crystallography, ^{57}Fe Mössbauer, EPR and UV-vis techniques in combination with DFT calculations [110]. The Fe-P bond lengths of μ -phosphido Fe(III)Fe(III) and Fe(IV)Fe(IV) complexes, 1.993/1.999 and 2.002/2.008 Å, respectively, are significantly longer than those of μ -oxo and μ -nitrido complexes. The Mössbauer parameters of μ -phosphido Fe(III)Fe(III) complex ($\delta = 0.01\text{mm s}^{-1}$, $\Delta E_Q = 1.94\text{ mm s}^{-1}$) are very close to those of μ -oxo counterpart ($\delta = 0.04\text{mm s}^{-1}$, $\Delta E_Q = 2.56\text{ mm s}^{-1}$) [111]. Noteworthy, the value of the isomeric shift is almost insensitive to the oxidation state of diiron site (Fig. 33). Careful electrochemical and spectroscopic studies indicated the retention of binuclear Fe-(μ P)-Fe structure upon the change of the iron oxidation states. Such rich redox properties of the stable μ -phosphido diiron complex suggest a possible evaluation of the catalytic properties of this rare scaffold.

The treatment of the same Fe(III) NHC complex with S_8 resulted in the formation of a trans-1,2 end-on disulfide-bridged diiron species (Fig. 34).

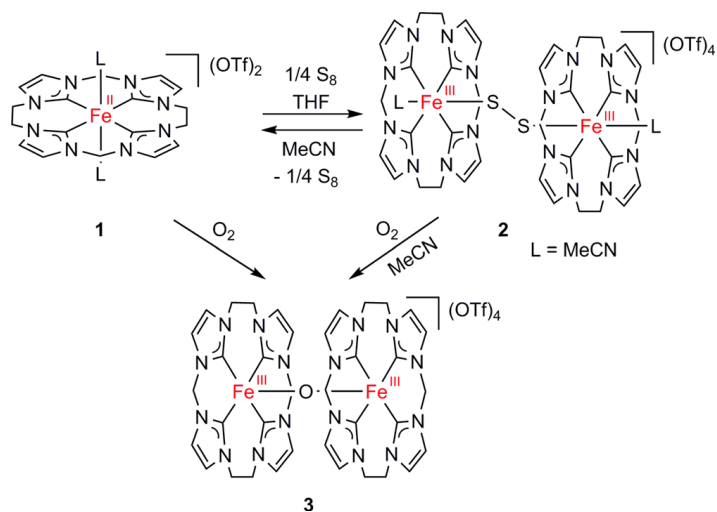


Fig. 34. Preparation of disulfide-bridged diiron complex with macrocyclic tetracarbene ligands.

Reprinted with permission from ref. 112. Copyright (2015) American Chemical Society.

This complex with strong σ -donating ligands and extremely strong antiferromagnetic coupling ($-J > 800 \text{ cm}^{-1}$) between two low-spin Fe(III) centers is quite labile in solution which make difficult the evaluation of its catalytic properties.

4.6. Miscellaneous μ -bridging groups

A stable μ -hyponitrite-bridged diiron porphyrin complex (OEP)Fe^{III}- μ ONNO-Fe^{III}(OEP) (OEP = octaethylporphyrin) was obtained by the treatment of corresponding μ -oxo complex with hyponitrous acid H₂N₂O₂ [113]. The distance between the two high-spin Fe centers in Fe-O-N=N-O-Fe unit (Fe-O = 1.889 Å, O-N = 1.375 Å, N-N = 1.250 Å) is 6.7 Å. Further studies showed that the electronic structure of this complex as well as (PPDME)Fe^{III}- μ ONNO-Fe^{III}(PPDME) (PPDME = protoporphyrin dimethyl ester) is better described as having two intermediate-spin ($S = 3/2$) Fe sites which are weakly antiferromagnetically coupled across μ -ONNO bridge [114].

The stable μ -N₂ diosmium salen complexes [(X)(salen)Os^{II}-NN-Os^{III}(salen)(X)](PF₆) and [(X)(salen)Os^{III}-NN-Os^{III}(salen)(X)](PF₆)₂ (X = 4-^tBupy or 4-MeTz) have also been described [115].

μ -Fluoro diiron(III) bisporphyrins exhibit a bent Fe-F-Fe fragment (151.6 - 153.6°) with quite long Fe-F bonds (1.931 – 1.944 Å) and weak antiferromagnetic coupling between two Fe(III) sites ($J =$ from -33 to -40 cm^{-1}) [116]. In contrast to μ -hydroxo counterparts [96], the Fe(III) sites in μ -fluoro species are equivalent. A family of bisporphyrins where two Fe(III) centers are bridged by the dianions of hydroquinones has been described [117].

Macrocyclic N-heterocyclic carbene ligands which are strong σ -donors structurally similar to but electronically distinct from porphyrins can also be used to construct μ -nitrido dimetal platform. The treatment of Cr(II) complex with Me₃SiN₃ afforded the first linearly μ -nitrido bridged Cr(III)Cr(IV) complex with a 50 % yield (Fig. 35) [118].

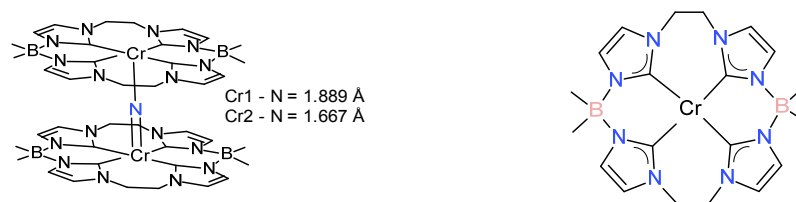


Fig. 35. μ -Nitrido dichromium (III,IV) complex supported by macrocyclic carbene ligands with non-equivalent Cr- μ N bonds.

The X-ray structural data indicated a linear asymmetric $\text{Cr}^{\text{III}}-\mu\text{N}=\text{Cr}^{\text{IV}}$ fragment with nonequivalent metal sites and distorted macrocyclic ligands. Magnetic susceptibility data suggest weak ferromagnetic coupling between Cr(III) and Cr(IV) centers [118].

4.7. Mixed μ -nitrido porphyrin – non-heme complexes

A series of heterobimetallic heteroleptic μ -nitrido complexes $[(\text{L})(\text{por})\text{M}-\mu\text{N}-\text{M}'(\text{LOEt})\text{Cl}_2]$ where por = 5,10,15,20-tetraphenylporphyrin or 5,10,15,20-tetra(p-tolyl)porphyrin; $\text{LOEt}^- = [\text{Co}(\eta^5-\text{C}_5\text{H}_5)\{\text{P}(\text{O})(\text{OEt})_2\}]^-$; M = Fe, Ru or Os; M' = Ru or Os; L = H₂O or pyridine have been prepared (Fig. 36) [119].

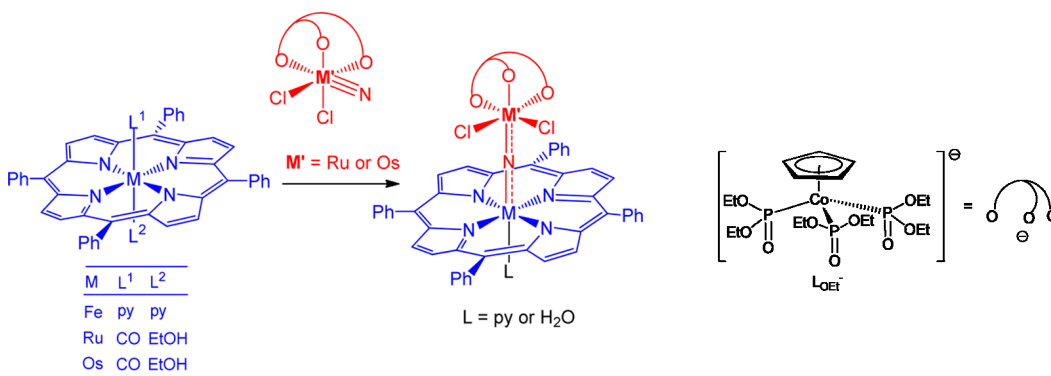


Fig. 36. μ -Nitrido heterobimetallic (Fe, Ru, Os) heteroleptic complexes. Reprinted with permission from ref. 119. Copyright (2017) American Chemical Society.

The diamagnetism and short (por)M- μ N bond lengths (Fe-N = 1.683 Å; Ru-N = 1.743 Å) are in agreement with $\text{M}^{\text{IV}}=\text{N}=\text{M}'^{\text{IV}}$ bonding description. Cyclic voltammetry showed a strong dependence of redox potentials on the nature of the metal sites suggesting that appropriate metal

combinations might provide a possibility to reach high-valent oxidation states which could be suitable for catalysis.

The versatility of the electrophilic $[\text{LOEtRu}^{\text{VI}}\equiv\text{N}(\text{Cl})_2]$ complex as nitride donor for synthesis of μ -nitrido heterometallic complexes was further demonstrated by preparation of $[\text{R}(\text{TPP})\text{Ir}-\mu\text{N}-\text{RuCl}_2(\text{LOEt})]$ with R = alkyl group [120]. The oxidation of this complex by $[\text{N}(4\text{-BrC}_6\text{H}_4)_3](\text{SbCl}_6)$ led to the Ir-C bond cleavage and formation of the chloride complex $[\text{Cl}(\text{TPP})\text{Ir}-\mu\text{N}-\text{RuCl}_2(\text{LOEt})]$. The short μN -Ir distances in $[\text{R}(\text{TPP})\text{Ir}-\mu\text{N}-\text{RuCl}_2(\text{LOEt})]$ (1.944 Å) and $[\text{Cl}(\text{TPP})\text{Ir}-\mu\text{N}-\text{RuCl}_2(\text{LOEt})]$ (1.831 Å) indicate multiple bonds and these species can be described by the two resonance structures: $\text{Ir}^{\text{III}}-\text{N}\equiv\text{Ru}^{\text{VI}}$ and $\text{Ir}^{\text{V}}=\text{N}=\text{Ru}^{\text{IV}}$. Although Ir^{IV} complexes are promising catalysts in several organic reactions, Ir porphyrins in high oxidation states (IV or higher) are still rare. These unprecedented high-valent Ir porphyrins connected to high-valent Ru via μ -nitrido group would be interesting to evaluate in catalysis.

The same synthetic strategy was used for the preparation of heteroleptic heterometallic phthalocyanine complexes with $\text{Ru}(\text{IV})\mu\text{NFe}(\text{IV})$ unit [121]. The treatment of $\text{Fe}^{\text{II}}\text{Pc}$ with $\text{Ru}^{\text{VI}}\equiv\text{N}(\text{LOEt})\text{Cl}_2$ furnished $[\text{Cl}_2(\text{LOEt})\text{Ru}^{\text{IV}}-\mu\text{N})-\text{Fe}^{\text{IV}}\text{Pc}(\text{H}_2\text{O})]$ with Ru-N-Fe angle of 176.0° and Fe-N and Ru-N distances of 1.677 and 1.689 Å, respectively. The oxidation of $[\text{Cl}_2(\text{LOEt})\text{Ru}^{\text{IV}}-\mu\text{N})-\text{Fe}^{\text{IV}}\text{Pc}(\text{H}_2\text{O})]$ with $[\text{N}(4\text{-BrC}_6\text{H}_4)_3](\text{SbCl}_6)$ and PhICl_2 resulted in the formation of corresponding $\text{Ru}(\text{IV})\text{Fe}(\text{IV})$ phthalocyanine cation-radical complexes (Fig. 37).

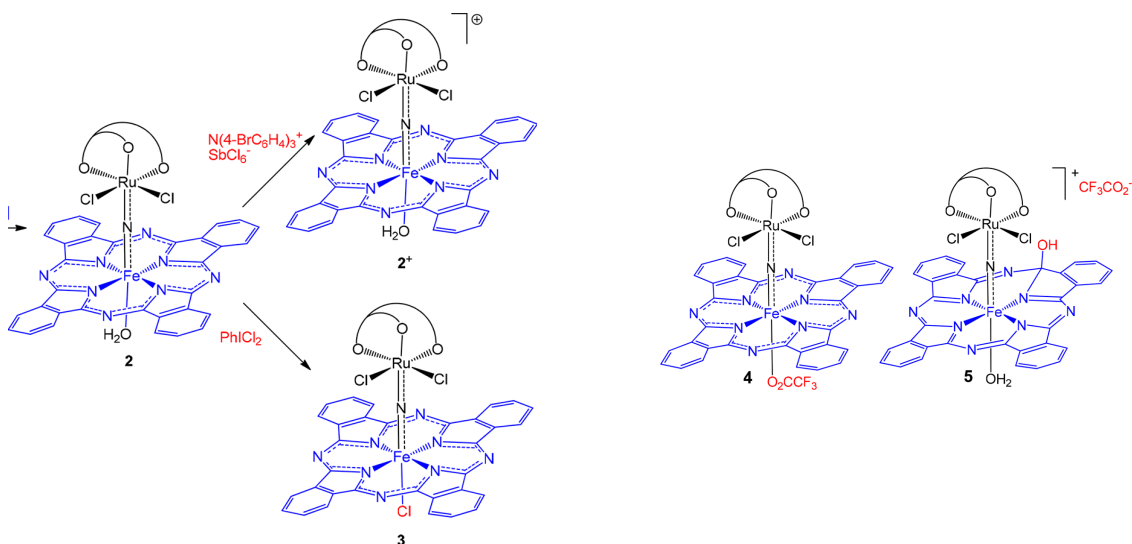


Fig. 37. Structures of the heteroleptic heterometallic phthalocyanine complex with Ru(IV) μ NFe(IV) unit and its oxidation to the cation-radical species using different oxidants. Adapted with permission from ref. 121. Copyright (2018) American Chemical Society.

Noteworthy, the reaction with PhI(CF₃COO)₂ led to the insertion of hydroxo group into Pc moiety (Fig. 37) [121]. The ability of heterometallic Ru^{IV}/Fe^{IV} μ -nitrido complex to access higher oxidation states and the hydroxylation of phthalocyanine cycle suggest possible oxidative reactivity of these interesting compounds.

5. Conclusion

About 25 years ago we have introduced water-soluble iron phthalocyanine complexes as catalysts for oxidative degradation of recalcitrant pollutants [7-11]. Since then, the scope of catalytic applications of phthalocyanine complexes has been greatly increased [27]. The recent trend is the increasing use of mononuclear phthalocyanine complexes in catalysis for the preparation of elaborated organic compounds [122-128].

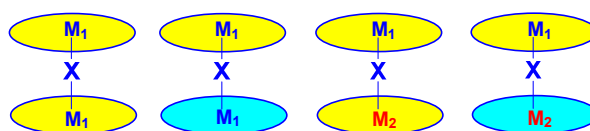
The introduction of binuclear complexes as catalysts has opened a new area and significantly enlarged a reaction scope with novel reactivities. We showed that μ -nitrido diiron construction is very suitable for obtaining active oxo and peroxo diiron species and their involvement in the oxidation reactions was demonstrated [60,61]. The particular electronic structures of these μ -nitrido diiron based species confer them unusual reactivity in challenging reactions such as the oxidation of methane and oxidative defluorination of heavily fluorinated aromatic compounds. Not surprisingly that the electronic structures of these μ -nitrido bridged diiron species have been a subject of extensive computational studies [64-67,82,129-131].

Along with fundamental studies of single-atom bridged bimetallic porphyrinoid complexes, the development of industrially relevant processes can be envisaged. For instance, a large scale production and application of fluorinated compounds as well as their extraordinary inertness to biodegradation result in their accumulation in environment including ground water.

Consequently, the development of disposal methods for these compounds is of great importance, since biodegradability of even partially fluorinated xenobiotics is very low and they are also very recalcitrant to traditional dépollution methods. μ -Nitrido diiron phthalocyanines are efficient practical catalysts for the oxidative degradation of chlorinated phenols and heavily fluorinated aromatic compounds in water with hydrogen peroxide, cheap and clean industrial oxidant. *N*-Bridged diiron phthalocyanine complexes are stable, non-toxic, non-expensive and available on a large scale. They can be readily immobilized onto different supports via covalent anchoring or electrostatic interaction. For all these reasons, we believe that the further development of this catalytic system might lead to practical industrially relevant method for disposal of these recalcitrant pollutants of emerging concern.

μ -Nitrido diiron phthalocyanine can find other applications. For instance, alkylthio-tetrasubstituted complexes combined with lutetium bis-phthalocyanine form heterojunctions showing a high sensitivity to ammonia, with a very good signal/noise ratio, at ambient temperature and atmospheric conditions [132].

Further development of the single-atom bridged macrocyclic metal complexes should provide new possibilities. Indeed, a great variety of homo- and heterometallic complexes in homoleptic or heteroleptic arrangement can be prepared (Fig. 38) and their properties can be adjusted using different porphyrin-like macrocycles with electron-withdrawing or electron-donating groups.



M_1 and $M_2 = \text{Fe, Mn, Cr, V, Ru, Os, Ir...}$
 $X = \text{O, N, C, P...}$

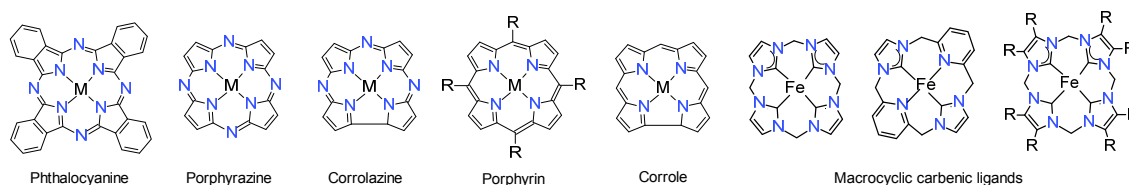


Fig. 38. Flexibility of μ -nitrido binuclear macrocyclic platform: access to homometallic and heterometallic complexes in homoleptic or heteroleptic arrangement involving macrocyclic ligands.

The development of μ -nitrido diiron complexes via modification of the structure of the macrocyclic ligand(s) is a tool which should open new possibilities for catalytic applications. For example, phthalocyanine complexes with electron-withdrawing [133] and electron-donating substituents [134] as well as the first water-soluble μ -nitrido diiron tetrasulfophthalocyanine [135] to provide the possibility to use these promising catalysts in water have been prepared.

The structural simplicity and flexibility of single-atom bridged porphyrin-like complexes make them promising catalysts for a variety of reactions. This bimetallic platform has a significant potential for further evolution. Different macrocyclic ligands including phthalocyanines, porphyrazines, porphyrins and probably corrolazines, corroles, etc. can be used to accommodate homometallic and heterometallic M-X-M units with different transition metals and bridging groups. Provided that challenges in the synthesis of these complexes can be overcome, a variety of homoleptic and heteroleptic structures may be prepared. The structural modification should significantly affect their electronic structure and this strategy can be used to tune their catalytic properties to develop tailored catalysts for a variety of reactions. We hope that unusual properties of μ -nitrido diiron phthalocyanine and porphyrin complexes will stimulate further research to discover new possibilities in the application of this novel tool in catalysis.

5. Acknowledgements

The author is grateful to all coworkers and collaborators whose names are given in the references for their important contributions to the development of μ -chemistry. Dr. E.V. Kudrik and Dr. P. Afanasiev are particularly acknowledged for the fruitful collaboration and stimulating discussions. Research support was provided by Agence Nationale de Recherches (ANR, France,

grants ANR-08-BLANC-0183-01, ANR-14-CE07-0018, ANR-16-CE29-0018-01), by CNRS (PICS project 6295) and by Région Rhône-Alpes.

6. References

- [1] X. Huang, J.T. Groves, *Chem. Rev.* 118 (2018) 2491-2553.
- [2] M. Costas, *Coord. Chem. Rev.* 255 (2011) 2912-2932.
- [3] X.P. Zhang, H. Lu, *Chem. Soc. Rev.* 40 (2011) 1899-1909.
- [4] D. Intrieri, D.M. Carminati, E. Gallo, Recent advances in metal porphyrinoid-catalyzed nitrene and carbene transfer reactions, in *Handbook of Porphyrin Science*, eds. K.M. Kadish, K.M. Smith, R. Guilard, World Scientific, Singapore, 2016, vol 38, pp 1-99.
- [5] R.F. Parton, I.F.J. Vankelecom, M.J.A. Casselman, C.P. Bezoukhanova, J.B. Uytterhoeven, P.A. Jacobs, *Nature* 370 (1994) 541-544.
- [6] L. Aviv-Harel, Z. Gross, *Chem. Eur. J.* 15 (2009) 8382-8394.
- [7] A. Sorokin, J.-L. Séris, B. Meunier, *Science* 268 (1995) 1163-1166.
- [8] A. Sorokin, B. Meunier, *Chem. Eur. J.* 2 (1996) 1308-1317.
- [9] A. Sorokin, S. De Suzzoni-Dezard, D. Poullain, J.-P. Noël, B. Meunier, *J. Am. Chem. Soc.* 118 (1996) 7411-7412.
- [10] B. Meunier, A. Sorokin, *Acc. Chem. Res.* 30 (1997) 470-476.
- [11] A. Sorokin, L. Fraisse, A. Rabion, B. Meunier, *J. Mol. Catal. A* 117 (1997) 103-114.
- [12] A. Sorokin, B. Meunier, *Eur. J. Inorg. Chem.* (1998) 1269-1281.
- [13] K. Pirkanniemi, M. Sillanpää, A. Sorokin, *Sci. Total Environ.* 307 (2003) 11-18.
- [14] M. Sanchez, N. Chap, J.P. Cazaux, B. Meunier, *Eur. J. Inorg. Chem.* (2001) 1775-1783.
- [15] M. Sanchez, A. Hadasch, A. Rabion, B. Meunier, *C. R. Chimie* (1999) 241-250.
- [16] K. Ozoemena, N. Kuznetsova, T. Nyokong, *J. Mol. Catal. A* 176 (2001) 29-40.
- [17] M. Sanchez, A. Hadasch, R.T. Fell, B. Meunier, *J. Catal.* 202 (2001) 177-186.
- [18] K. Ozoemena, N. Kuznetsova, T. Nyokong, *J. Photochem. Photobiol. A* 139 (2001) 217-224.

- [19] T.B. Ogunbayo, T. Nyokong, *J. Mol. Catal. A: Chem.* 350 (2011) 49-55.
- [20] D. Wöhrle, O. Suvorova, R. Gerdes, O. Bartels, L. Lapok, N. Baziakina, S. Makarov, A. Slodek, *J. Porphyrins Phthalocyanines* 8 (2004) 1020-1041.
- [21] B. Agboola, K.I. Ozoemena, T. Nyokong, *J. Mol. Catal. A: Chem.* 227 (2005) 209-216.
- [22] X. Tao, W. Ma, T. Zhang, J. Zhao, *Chem. Eur. J.* 8 (2002) 1321-1326.
- [23] X. Tao, W. Ma, T. Zhang, J. Zhao, *Angew. Chem. Int. Ed.* 40 (2001) 3014-3016.
- [24] N. Nensala, T. Nyokong, *J. Mol. Catal. A: Chem.* 164 (2000) 69-76.
- [25] Z. Xiong, Y. Xu, L. Zhu, J. Zhao, *Langmuir* 21 (2005) 10602-10607.
- [26] T. Ichinohe, H. Miyasaka, A. Isoda, M. Kimura, K. Hanabusa, H. Shirai, *React. Func. Polym.* 43 (2000) 63-70.
- [27] A.B. Sorokin, *Chem. Rev.* 113 (2013) 8152-8191.
- [28] A.B. Sorokin, E.V. Kudrik, *Catal. Today* 159 (2011) 37-46.
- [29] P. Afanasiev, E.V. Kudrik, F. Albrieux, V. Briois, O.I. Koifman, A.B. Sorokin, *Chem. Commun.* 48 (2012) 6088-6090.
- [30] S.L. Kachkarova-Sorokina, P. Gallezot, A.B. Sorokin, *Chem. Commun.* (2004) 2844-2845.
- [31] A.B. Sorokin, S.L. Kachkarova-Sorokina, C. Donzé, C. Pinel, P. Gallezot, *Top. Catal.* 27 (2004) 67-76.
- [32] A.B. Sorokin, A. Tuel, *New J. Chem.* 23 (1999) 473-476.
- [33] C. Pergrale, A.B. Sorokin, *C.R. Chimie* 3 (2000) 803-810.
- [34] I.M. Geraskin, O. Pavlova, H.M. Neu, M.S. Yusupov, V.N. Nemykin, V.V. Zhdankin, *Adv. Synth. Catal.* 351 (2009) 733-737.
- [35] H.M. Neu, V.V. Zhdankin, V.N. Nemykin, *Tetrahedron Lett.* 51 (2010) 6545-6548.
- [36] H.M. Neu, M.S. Yusupov, V.V. Zhdankin, V.N. Nemykin, *Adv. Synth. Catal.* 351 (2009) 3168-3174.
- [37] C. Pérollier, C. Pergrale-Mejean, A.B. Sorokin, *New J. Chem.* 29 (2005) 1400-1403.

- [38] O.V. Zalomaeva, I.D. Ivanchikova, O.A. Kholdeeva, A.B. Sorokin, *New J. Chem.* 33 (2009) 1031-1037.
- [39] O.V. Zalomaeva, A.B. Sorokin, *New J. Chem.* 30 (2006) 1768-1773.
- [40] D.A. Summerville, I.A. Cohen, *J. Am. Chem. Soc.* 98 (1976) 1747-1752.
- [41] D.F. Bocian, E.W. Finsden, J.A. Hofmann, G.A. Schick, D.R. English, D.N. Hendrickson, K.S. Suslick, *Inorg. Chem.* 23 (1984) 800-807.
- [42] V.L. Goedken, C. Ercolani, *J. Chem. Soc. Chem. Commun.* (1984) 378-379.
- [43] L.A. Bottomley, J.-N. Gorce, V.L. Goedken, C. Ercolani, *Inorg. Chem.* 24 (1985) 3733-3737.
- [44] P.A. Stuzhin, L. Latos-Grazynski, A. Jezierski, *Trans. Met. Chem.* 14 (1989) 341-346.
- [45] P.A. Stuzhin, M. Hamdush, H. Homborg, *Mendeleev Commun.* 7 (1997) 196-198.
- [46] C. Ercolani, S. Hewage, R. Heucher, G. Rossi, *Inorg. Chem.* 32 (1993) 2975-2977.
- [47] C. Ercolani, J. Jubb, G. Pennesi, U. Russo, G. Trigiane, *Inorg. Chem.* 34 (1995) 2535-2541.
- [48] M.P. Donzello, C. Ercolani, K.M. Kadish, Z. Ou, U. Russo, *Inorg. Chem.* 37 (1998) 3682-3688.
- [49] B. Floris, M.P. Donzello, C. Ercolani, Single-Atom Bridged Dinuclear Metal Complexes with Emphasis on Phthalocyanine System. In *The Porphyrin Handbook*; K.M. Kadish, K.M. Smith, R. Guilard, Eds., Academic Press: Amsterdam, 2003, Vol. 18, p 1-62.
- [50] E.V. Kudrik, O. Safonova, P. Glatzel, J.C. Swarbrick, L.X. Alvarez, A.B. Sorokin, P. Afanasiev, *Appl. Catal. B* 113-114 (2012) 43-51.
- [51] A.B. Sorokin, E.V. Kudrik, D. Bouchu, *Chem. Commun.* (2008) 2562-2564.
- [52] A.B. Sorokin, E.V. Kudrik, L.X. Alvarez, P. Afanasiev, J.M.M. Millet, D. Bouchu, *Catal. Today* 157 (2010) 149-154.
- [53] E.V. Kudrik, A.B. Sorokin, *Chem. Eur. J.* 14 (2008) 7123-7126.
- [54] P. Afanasiev, D. Bouchu, E.V. Kudrik, J.M.M. Millet, A.B. Sorokin, *Dalton Trans.* (2009) 9828-9836.

- [55] Ü. İşci, P. Afanasiev, J.M.M. Millet, E.K. Kudrik, V. Ahsen, A.B. Sorokin, Dalton Trans. (2009) 7410-7420.
- [56] P. Afanasiev, E.V. Kudrik, J.M.M. Millet, D. Bouchu, A.B. Sorokin, Dalton Trans. 40 (2011) 701-710.
- [57] [] L.X. Alvarez, E.V. Kudrik, A.B. Sorokin, Chem. Eur. J. 17 (2011) 9298-9301.
- [58] E.V. Kudrik, P. Afanasiev, D. Bouchu, J.M.M. Millet, A.B. Sorokin, J. Porphyrins Phthalocyanines 12 (2008) 1078-1089.
- [59] C. Colombar, E.V. Kudrik, P. Afanasiev, A.B. Sorokin, J. Am. Chem. Soc. 136 (2014) 11321-11330.
- [60] P. Afanasiev, A.B. Sorokin, Acc. Chem. Res. 49 (2016) 583-593.
- [61] A.B. Sorokin, Adv. Inorg. Chem. 70 (2017) 107-169.
- [62] Ü. İşci, F. Dumoulin, A.B. Sorokin, V. Ahsen, Turk. J. Chem. 38 (2014) 923-949.
- [63] E.V. Kudrik, P. Afanasiev, L.X. Alvarez, P. Dubourdeaux, M. Clémancey, J.-M. Latour, G. Blondin, D. Bouchu, F. Albrieux, S.E. Nefedov, A.B. Sorokin, Nature Chem. 4 (2012) 1024-1029.
- [64] Ü. İşci, A.S. Faponle, P. Afanasiev, F. Albrieux, V. Briois, V. Ahsen, F. Dumoulin, A.B. Sorokin, S.P. de Visser, Chem. Sci. 6 (2015) 5063-5075.
- [65] C. Colombar, E.V. Kudrik, V. Briois, J.C. Swarbrick, A.B. Sorokin, P. Afanasiev, Inorg. Chem. 53 (2014) 11517-11530.
- [66] M.G. Quesne, D. Senthilnathan, D. Singh, D. Kumar, P. Maldivi, A.B. Sorokin, S.P. de Visser, ACS Catal. 6 (2016) 2230-2243.
- [67] M.Q.E. Mubarak, A.B. Sorokin, S.P. de Visser, J. Biol. Inorg. Chem. 24 (2019) 1127-1134.
- [68] L.X. Alvarez, A.B. Sorokin, J. Organomet. Chem. 793 (2015) 139-144.
- [69] Y. Yamada, K. Morita, N. Mihara, K. Igawa, K. Tomooka, K. Tanaka, New J. Chem. 43 (2019) 11477-11482.

- [70] N. Mihara, Y. Yamada, H. Takaya, Y. Kitagawa, K. Igawa, K. Tomooka, H. Fujii, K. Tanaka, *Chem. Eur. J.* 25 (2019) 3369-3375.
- [71] S.V. Zaitseva, O.R. Simonova, S.A. Zdanovich, E.V. Kudrik, O.I. Koifman, *Macroheterocycles* 7 (2014) 55-59.
- [72] E.V. Kudrik, A.B. Sorokin, *J. Mol. Catal. A: Chem.* 426 (2017) 499-505.
- [73] K. Seo, H. Kim, J. Lee, M.-G. Kim, S.-Y. Seo, C. Kim, *J. Ind. Eng. Chem.* 53 (2017) 371-374.
- [74] K. Cho, H. Kim, L.M. Nhut, K. Seo, M.-G. Kim, C. Kim, *Chem. Eng. Res. Des.* 144 (2019) 429-433.
- [75] S.P. de Visser, S. Shaik, *J. Am. Chem. Soc.* 125 (2003) 7413-7424.
- [76] N.V. Tkachenko, R.V. Ottenbacher, O.Y. Lyakin, A.M. Zima, D.G. Samsonenko, E.P. Talsi, K.P. Bryliakov, *ChemCatChem*. 10 (2018) 4052-4057.
- [77] D.R. Boyd, N.D. Sharma, *Chem. Soc. Rev.* 25 (1996) 289-296.
- [78] C. Bleasdale, R. Cameron, C. Edwards, B.T. Golding, *Chem. Res. Toxicol.* 10 (1997) 1314-1318.
- [79] C. Colombari, E.V. Kudrik, P. Afanasiev, A.B. Sorokin, *Catal. Today* 235 (2014) 14-19.
- [80] A.S. Makarova, E.V. Kudrik, S.V. Makarov, O.I. Koifman, *J. Porphyrins Phthalocyanines* 18 (2014) 604-613.
- [81] C. Colombari, A.B. Sorokin, *J. Coord. Chem.* 71 (2018) 1814-1821.
- [82] C. Colombari, A.H. Tobing, G. Mukherjee, C.V. Sastri, A.B. Sorokin, S.P. de Visser, *Chem. Eur. J.* 25 (2019) 14320-14331.
- [83] A.B. Sorokin, *Coord. Chem. Rev.* 389 (2019) 141-160.
- [84] C. Colombari, E.V. Kudrik, D.V. Tyurin, F. Albrieux, S.E. Nefedov, P. Afanasiev, A.B. Sorokin, *Dalton Trans.* 44 (2015) 2240-2251.
- [85] L.P. Cailler, M. Clémancey, J. Barilone, P. Maldivi, J.-M. Latour, A.B. Sorokin, *Inorg. Chem.* 59 (2020) 1104-1116.

- [86] Y. Zhang, *Chem. Eur. J.* 25 (2019) 13231-13247.
- [87] M.R. Anneser, S. Haslinger, A. Pöthig, M. Cokoja, V. D'Elia, M.P. Högerl, J.-M. Basset, F.E. Kühn, *Dalton Trans.* 45 (2016) 6449-6455.
- [88] C. Cordes (née Kupper), M. Morganti, I. Klawitter, L. Schremmer, S. Dechert, F. Meyer, *Angew. Chem. Int. Ed.* 58 (2019) 10855-10858.
- [89] D. Sil, F.S.T. Khan, S.P. Rath, *Chem. Eur. J.* 22 (2016) 14585-14597.
- [90] D. Sil, S. Bhowmik, F.S.T. Khan, S.P. Rath, *Inorg. Chem.* 55 (2016) 3239-3251.
- [91] M.A. Sainna, D. Sil, D. Sahoo, B. Martin, S.P. Rath, P. Comba, S.P. de Visser, *Inorg. Chem.* 54 (2015) 1919-1930.
- [92] D. Sil, S.P. Rath, *Dalton Trans.* 44 (2015) 16195-16211.
- [93] D. Sil, F.S.T. Khan, S.P. Rath, *Inorg. Chem.* 53 (2014) 11925-11936.
- [94] S. Bhowmik, S.K. Ghosh, S. Layek, H.C. Verna, S.P. Rath, *Chem. Eur. J.* 18 (2012) 13025-13037.
- [95] S.K. Ghosh, R. Patra, S.P. Rath, *Inorg. Chem.* 49 (2010) 3449-3460.
- [96] T. Guchhait, S. Sasmal, F.S.T. Khan, S.P. Rath, *Coord. Chem. Rev.* 337 (2017) 112-144.
- [97] J. Rosenthal, J. Bachman, J.L. Dempsey, A.J. Esswein, T.G. Gray, J.M. Hodgkiss, D.R. Manke, T.D. Lockett, B.J. Pistorio, A.S. Veige, D.G. Nocera, *Coord. Chem. Rev.* 249 (2005) 1316-1326.
- [98] F.S.T. Khan, T. Guchhait, S. Sasmal, S.P. Rath, *Dalton Trans.* 46 (2017) 1012-1037.
- [99] D. Lai, F.S.T. Khan, S.P. Rath, *Dalton Trans.* 47 (2018) 14388-14401.
- [100] O.R. Simonova, S.V. Zaitseva, E.Yu. Tyulyaeva, S.A. Zhdanovich, E.V. Kudrik, *Russ. J. Inorg. Chem.* 62 (2017) 508-518.
- [101] S.V. Zaitseva, E.Yu. Tyulyaeva, O.R. Simonova, S.A. Zhdanovich, D.V. Tyurin, O.I. Koifman, *J. Coord. Chem.* 71 (2018) 2993-3007.
- [102] S.V. Zaitseva, D.V. Tyurin, S.A. Zhdanovich, O.I. Koifman, *Russ. J. Inorg. Chem.* 64 (2019) 815-821.

- [103] D.V. Tyurin, S.V. Zaitseva, E.V. Kudrik, *Russ. J. Phys. Chem.* 92 (2018) 870-875.
- [104] O.R. Simonova, S.V. Zaitseva, S.A. Zhdanovich, O.I. Koifman, *Macroheterocycles* 11 (2018) 29-34.
- [105] O.R. Simonova, S.V. Zaitseva, E.Yu. Tyulyaeva, S.A. Zhdanovich, O.I. Koifman, *Russ. J. Phys. Chem. A* 92 (2018) 2128-2134.
- [106] S.V. Zaitseva, E.Yu. Tyulyaeva, S.A. Zhdanovich, O.I. Koifman, *J. Mol. Liq.* 287 (2019) 111023.
- [107] A. Kienast, L. Galich, K.S. Murray, B. Moubaraki, G. Lazarev, J.D. Cashion, H. Homborg, *J. Porphyrins Phthalocyanines* 1 (1997) 141-157.
- [108] A.P. Kroitor, L.P. Cailler, A.G. Martynov, Yu.G. Gorbunova, A.Yu. Tsivadze, A.B. Sorokin, *Dalton Trans.* 46 (2017) 15651-15655.
- [109] A.P. Kroitor, A.G. Martynov, Yu.G. Gorbunova, A.Yu. Tsivadze, A.B. Sorokin, *Eur. J. Inorg. Chem.* (2019) 1923-1931.
- [110] M. Ghosh, H.H. Cramer, S. Dechert, S. Demeshko, M. John, M.M. Hansmann, S. Ye, F. Meyer, *Angew. Chem. Int. Ed.* 58 (2019) 14349-14356.
- [111] S. Meyer, I. Klawitter, S. Demeshko, E. Bill, F. Meyer, *Angew. Chem. Int. Ed.* 52 (2013) 901-905.
- [112] S. Meyer, O. Krahe, C. Kupper, I. Klawitter, S. Demeshko, E. Bill, F. Neese, F. Meyer, *Inorg. Chem.* 54 (2015) 9770-9776.
- [113] N. Xu, L.O. Campbell, D.R. Powell, J. Khandogin, G.B. Richter-Addo, *J. Am. Chem. Soc.* 131 (2009) 2460-2461.
- [114] T.C. Berto, N. Xu, S.R. Lee, A.J. McNeil, E.E. Alp, J. Zhao, G.B. Richter-Addo, N. Lehnert, *Inorg. Chem.* 53 (2014) 6398-6414.
- [115] W.-L. Man, G. Chen, S.-M. Yiu, L. Shek, W.-Y. Wong, W.-T. Wong, T.-C. Lau, *Dalton Trans.* 39 (2010) 11163-11170.
- [116] D. Sil, A. Kumar, S.P. Rath, *Chem. Eur. J.* 22 (2016) 11214-11223.

- [117] D. Sahoo, A.K. Singh, S.P. Rath, *Eur. J. Inorg. Chem.* (2016) 3305-3313.
- [118] G.R. Elpitiya, B.J. Malbrecht, D.M. Jenkins, *Inorg. Chem.* 56 (2017) 14101-14110.
- [119] W.-M. Cheung, W.-H. Chiu, M. de Vere-Tucker, H.H.-Y. Sung, I.D. Williams, W.-H. Leung, *Inorg. Chem.* 56 (2017) 5680-5687.
- [120] S.-C. So, W.-M. Cheung, W.-H. Chiu, M. de Vere-Tucker, H.H.-Y. Sung, I.D. Williams, W.-H. Leung, *Dalton Trans.* 48 (2019) 8340-8349.
- [121] W.-M. Cheung, W.-M. Ng, W.-H. Wong, H.K. Lee, H.H.-Y. Sung, I.D. Williams, W.-H. Leung, *Inorg. Chem.* 57 (2018) 9215-9222.
- [122] J.R. Clark, K. Feng, A. Sookezian, M.C. White, *Nat. Chem.* 10 (2018) 583-591.
- [123] S.M. Paradine, J.R. Griffin, J. Zhao, A.L. Petronico, S.M. Miller, M.C. White, *Nat. Chem.* 7 (2015) 987-994.
- [124] H. Yu, Z. Li, C. Bolm, *Angew. Chem. Int. Ed.* 57 (2018) 12053-12056.
- [125] J.R. Griffin, C.I. Wendel, J.A. Garwin, M.C. White, *J. Am. Chem. Soc.* 139 (2017) 13624-13627.
- [126] D. Hirose, M. Gazvoda, J. Košmrlj, T. Taniguchi, *Chem. Sci.* 7 (2016) 5148-5159.
- [127] L. Legnani, B. Morandi, *Angew. Chem. Int. Ed.* 55 (2016) 2248-2251.
- [128] K. Yamaguchi, H. Kondo, J. Yamaguchi, K. Itami, *Chem. Sci.* 4 (2013) 3753-3757.
- [129] Q.M. Phung, K. Pierloot, *Chem. Eur. J.* 25 (2019) 12491-12498.
- [130] M. Ansari, N. Vyas, A. Ansari, G. Rajaraman, *Dalton Trans.* 44 (2015) 15232-15243.
- [131] R. Silaghi-Dumitrescu, S.V. Makarov, M.-M. Uta, I.A. Dereven'kov, P.A. Stuzhin, *New J. Chem.* 35 (2011) 1140-1145.
- [132] Z. Şahin, R. Meunier-Prest, F. Dumoulin, Ü. İşci, M. Bouvet, *Inorg. Chem.* 59 (2020) 1057-1067.
- [133] Ü. İşci, F. Dumoulin, V. Ahsen, A.B. Sorokin, *J. Porphyrins Phthalocyanines* 14 (2010) 324-334.

[134] E.V. Kudrik, P. Afanasiev, D. Bouchu, A.B. Sorokin, J. Porphyrins Phthalocyanines 15 (2011) 583-591.

[135] P.A. Stuzhin, S.S. Ivanova, I. Dereven'kov, S.V. Makarov, R. Silaghi-Dumitresku, H. Homborg, *Macroheterocycles* 5 (2012) 175-177.